Transcriptional profiling reveals potential involvement of microvillous TRPM5-expressing cells in viral infection of the olfactory epithelium

B. Dnate' Baxter[1,2,‡], Eric D. Larson[3 ‡], Laetitia Merle[1,2‡], Paul Feinstein[4], Arianna Gentile Polese[1,2], Andrew N. Bubak[5], Christy S. Niemeyer[5], James Hassell, Jr.[5], Doug Shepherd[6], Vijay R. Ramakrishnan[3], Maria A. Nagel[5], and Diego Restrepo[1,2,*]

[1]Neuroscience Graduate Program, University of Colorado Anschutz Medical Campus, Aurora, CO 80045, USA

[2]Department of Cell and Developmental Biology, University of Colorado Anschutz Medical Campus, Aurora, CO 80045, USA

[3]Department of Otolaryngology, University of Colorado Anschutz Medical Campus, Aurora, CO 80045, USA

[4]Department of Biological Sciences, Hunter College, CUNY, New York, NY, 10065, USA

[5]Department of Neurology, University of Colorado Anschutz Medical Campus, Aurora, CO 80045, USA

[6]Department of Pharmacology, University of Colorado Anschutz Medical Campus and Center for Biological Physics and Department of Physics, Arizona State University, USA

[‡]Co-first authors

[*]Corresponding author: Diego Restrepo, diego.restrepo@cuanschutz.edu

Abstract

Background: Understanding viral infection of the olfactory epithelium is essential because the olfactory nerve is an important route of entry for viruses to the central nervous system. Specialized chemosensory epithelial cells that express the transient receptor potential cation channel subfamily M member 5 (TRPM5) are found throughout the airways and intestinal epithelium and are involved in responses to viral infection.

Results: Herein we performed deep transcriptional profiling of olfactory epithelial cells sorted by flow cytometry based on the expression of mCherry as a marker for olfactory sensory neurons and for eGFP in OMP-H2B::mCherry/TRPM5-eGFP transgenic mice (*Mus musculus*). We find profuse expression of transcripts involved in inflammation, immunity and viral infection in TRPM5-expressing microvillous cells.

Conclusion: Our study provides new insights into a potential role for TRPM5-expressing microvillous cells in viral infection of the olfactory epithelium. We find that, as found for solitary chemosensory cells (SCCs) and brush cells in the airway epithelium, and for tuft cells in the intestine, the transcriptome of TRPM5-expressing microvillous cells indicates that they are likely involved in the inflammatory response elicited by viral infection of the olfactory epithelium.

Keywords: Olfactory sensory neurons, Microvillous cells, Viral infection, Immunity, Inflammation, Mouse

Background

Chemosensory cells found in the airway (SCCs/brush cells) and intestinal epithelium (tuft cells) express the transient receptor potential cation channel subfamily M member 5 (TRPM5) and other elements of the taste transduction pathway and have been implicated in immune and inflammatory responses to bacterial, viral and parasitic infection (Luo et al., 2019; Maina et al., 2018; O'Leary et al., 2019; Perniss et al., 2020; Rane et al., 2019; Saunders et al., 2014; Tizzano et al., 2010). In the olfactory epithelium TRPM5 and other proteins involved in taste transduction are also expressed in SCC-like microvillous cells (MVCs)(Genovese and Tizzano, 2018; Lin et al., 2008), which have been proposed to be involved in a protective response to high concentrations of odorants (Fu et al., 2018; Lemons et al., 2017). However, whether MVCs play a role in viral infection or viral infection defense of the olfactory epithelium is unknown.

Herein, we performed transcriptional profiling of MVCs and a subset of olfactory sensory neurons (OSNs) expressing eGFP under control of a fragment of the TRPM5 promoter (OSN_eGFP+ cells)(Lin et al., 2007; Lopez et al., 2014). In order to profile these low abundance cells we used a modified version of Probe-Seq, which allows deep transcriptional profiling of specific cell types identified by fluorescent markers as the defining feature (Amamoto et al., 2019). We crossed a mouse expressing mCherry in the nuclei of OSNs under control of the OMP promoter (OMP-H2B::mCherry mice) with TRPM5-eGFP transgenic mice (Clapp et al., 2006) (OMP-H2B::mCherry/TRPM5-eGFP mice). We isolated cells from the olfactory epithelium and used fluorescence-activated cell sorting (FACS) to sort MVC_eGFP cells (mCherry negative and eGFP positive) and cells labeled by OMP-driven mCherry that did or did not express eGFP

67 (OSN_eGFP+ and OSN_eGFP- cells) followed by transcriptional profiling by RNA sequencing

68 (RNAseq).

69

70

Results

Fluorescence-activated cell sorting of cells isolated from the main olfactory epithelium. The olfactory epithelium of OMP-H2B::mCherry/TRPM5-eGFP mice expressed nuclear mCherry driven by the OMP promoter in the intermediate layer of the olfactory epithelium (Figure 1a), as expected for the location of nuclei of mature OSNs (Farbman and Margolis, 1980). eGFP expression driven by the TRPM5 promoter was found in MVCs, with cell bodies located mostly in the apical layer of the epithelium (asterisks), and at lower expression levels in a subset of OSNs double-labeled with mCherry (Figure 1a), consistent with earlier publications (Lin et al., 2008; Lin et al., 2007).

We proceeded to isolate cells from the main olfactory epithelium of OMP-H2B::mCherry/TRPM5-eGFP mice (see Figure 1b, Methods and Figure 1 - figure supplement 1). Figure 1c shows two isolated OSNs with differential expression of eGFP. Using flow cytometry we found that fluorescence intensity of individual cells for mCherry and eGFP spanned several orders of magnitude (Figure 1d). We proceeded to sort three groups of cells under light scattering settings to exclude doublets: high mCherry-expressing cells with low and high eGFP fluorescence (presumably mature OSNs, these cells are termed OSN_eGFP- and OSN_eGFP+ cells respectively) and cells with low mCherry and high eGFP expression (MVC_eGFP, presumably MVCs). Reverse transcription quantitative PCR (RT-qPCR) showed that, as expected the OSN_eGFP- and OSN_eGFP+ cells have higher levels of OMP transcript than MVC_eGFP cells (Figure 1e,i), and OSN_eGFP+ cells and MVC_eGFP cells have higher levels of eGFP transcript compared to OSN_eGFP- cells (Figure 1e,ii). Furthermore, compared

to OSN_eGFP- cells both the MVC_eGFP cells and OSN_eGFP+ cells expressed higher levels of TRPM5 transcript (Figure 1e,iii) and choline acetyl transferase (ChAT)(Figure 1e,iv), a protein involved in acetylcholine neurotransmission that is expressed in MVCs (Ogura et al., 2011). The asterisks in Figure 1e denote significant differences tested with either t-test or ranksum with p-values below the p-value of significance corrected for multiple comparisons using the false discovery rate (pFDR)(Curran-Everett, 2000) (pFDR is 0.033 for OMP, 0.05 for TRPM5, 0.05 for EGFP and 0.03 for ChAT, n=8 for OMP OSN_eGFP-, 4 for OMP OSN_eGFP+ and 4 for MVC_eGFP cells).

RNAseq indicates that MVC_eGFP and OSN_eGFP- are distinct groups of chemosensory cells in the mouse olfactory epithelium. Differential gene expression analysis of the RNAseq data was used to compare MVC_eGFP and OSN_eGFP- sorted by FACS. Expression of 4386 genes was significantly higher in MVC_eGFP cells compared to OSN_eGFP- cells, and expression of 5630 genes was lower in MVC_eGFP cells (Figure 2a shows the most significantly upregulated or downregulated genes and Figure 2 – figure supplement 1 shows the entire list). A total of 1073 Olfr genes were included in the analysis (including pseudogenes). While 9 were expressed at higher levels in the MVC_eGFP population their expression levels was very low (<100 counts) and the difference was not statistically significant. On the contrary, transcripts for 550 olfactory receptors were significantly higher in OSN_eGFP- cells (Figure 2b and 2c). *Trpm5* and *eGFP* were among the top 10 genes whose transcription was higher in MVC_eGFP cells compared to OSN_eGFP- cells with 1471-fold and 75-fold differences respectively (Figure 2a). Interestingly, *Pou2f3*, a transcription factor important in differentiation of MVCs (Yamaguchi et al., 2014; Yamashita et al., 2017), is found within the top 10 upregulated genes found in MVC_eGFP cells compared to OSN_eGFP- (Figure 2a). In addition, transcripts for

chemosensory cell specific cytokine IL-25 and its receptor IL-17RB (Ualiyeva et al., 2020) were more highly expressed in MVC_eGFP (Figure 2 – figure supplement 1). Finally, *OMP* and *s100a5*, genes for two proteins expressed in mature OSNs (Farbman and Margolis, 1980; Fischl et al., 2014), were among the top 10 downregulated transcripts in MVC_eGFP cells compared to OSN_eGFP- cells (Figure 2a).

We compared expression of transcripts involved in taste transduction, canonical olfactory transduction, and non-canonical OSNs (Figure 2d). MVC_eGFP cells expressed genes involved in the taste transduction pathway as expected for chemosensory epithelial cells of the olfactory epithelium (Ualiyeva et al., 2020). In contrast, OSN_eGFP- expressed transcripts for markers of canonical OSNs such as OMP, BBS1 and 2 and proteins involved in the canonical olfactory transduction pathway. The non-canonical OSNs considered here included guanilyl-cyclase D (GC-D) OSNs (Juilfs et al., 1997), Trpc2 OSNs (Omura and Mombaerts, 2014) and Cav2.1 OSNs (Pyrski et al., 2018). OSN_eGFP- expressed low levels of *Cancna1a* encoding for Cav2.1 and *Trpc2*. OSN_eGFP- expressed higher levels of Trace amine-associated receptors (Liberles, 2015) than MVC_eGFP cells.

Perusal of these top differences suggested that these are distinct chemosensory cell types found in the olfactory epithelium. In order to perform a thorough analysis of the differences between these chemosensory cell groups we performed an analysis of gene ontology (GO) enrichment for lists of genes related to chemosensory perception and neuronal identity. When compared with OSN_eGFP- we found that MVC_eGFP cells were enriched for transcripts belonging to gene ontologies of sensory perception of sweet/umami taste (GO:0050916 and GO:0050917) (Figure

2e, Figure 2 - figure supplement 2, Figure 2 - figure supplement 3) which includes taste detection/transduction proteins that have been reported to be expressed in MVCs (Genovese and Tizzano, 2018; Hegg et al., 2010): *Gnat3*, encoding for gustducin, the G protein mediating sweet and umami taste transduction (McLaughlin et al., 1992), *Itpr3*, encoding for the inositol-1,4,5-triphosphate receptor type 3 and *Tas1r3*, encoding for a gustducin-coupled receptor involved in umami and sweet taste (Damak et al., 2003; Zhang et al., 2003). In contrast, OSN_eGFP- were enriched for transcripts involved in events required for an organism to receive an olfactory stimulus, convert it to a molecular signal, and recognize and characterize the signal (GO:0007608). Finally, enrichment of gene ontology lists for synaptic vesicle function were decreased for MVC_eGFP cells compared with OSN_eGFP- cells (Figure 2e). Results of this gene ontology analysis of chemosensation and synaptic vesicle function reinforces the finding that the two cell groups in this study are distinct chemosensory cell types of the olfactory epithelium. OSN_eGFP- cells differ from MVC_eGFP cells in expression of olfactory receptors, chemosensation and transcripts related to synaptic function as expected for an OSN.

Finally, a question that arises is how the transcriptional profile of the MVC_eGFP cells of this study compares to transcriptional profiling of chemosensory epithelial cells isolated from the respiratory and olfactory epithelia in mice expressing eGFP under control of the ChAT promoter (Ualiyeva et al., 2020). Figure 2 - figure supplement 4 shows comparisons of gene expression between MVC_eGFP and OSN_eGFP- cells of this study and ChAT-eGFP MVCs and ChAT-eGFP SCCs profiled in the respiratory epithelium in the study of Ualiyeva and co-workers (Ualiyeva et al., 2020). This comparison is of limited value due to the fact that gene profiling was performed in two separate studies. However, in this preliminary analysis we find that MVCs

from this study have similar transcription profiles to ChAT-eGFP MVCs and differ from ChAT-eGFP SCCs. For example, MVC_eGFP and ChAT-eGFP MVCs showed enhanced expression of transcripts such as *Il25* and *Fos* (Figure 2 - figure supplement 3). The similarity of transcriptional profiling argues that in this study MVC_eGFPs were not contaminated with SCCs consistent with the fact that in our study we isolated MVC_eGFP from olfactory epithelium dissected apart from the respiratory epithelium and that the density of MVCs in the OE is higher than the density of SCCs in the respiratory epithelium (Ualiyeva et al., 2020) decreasing the chance of contamination of OE MVCs by SCCs. Interestingly, *Ugt2a1* and *Ugt2a2*, transcripts for proteins involved in UDP synthesis were higher in MVC_eGFP than ChAT-eGFP MVCs suggesting differences between these cells (Figure 2 - figure supplement 3). In order to determine whether these similarities and differences between MVCs in our study and the study of Ualiyeva and co-workers are real it will be necessary to perform simultaneous RNAseq profiling of these two populations.

Gene ontology analysis finds enrichment of lists of viral-related, inflammation and immune transcripts in MVC_eGFP cells. SCCs, tuft and brush cells have been implicated in responses to bacterial and viral infection, immunity and inflammation (Luo et al., 2019; Maina et al., 2018; O'Leary et al., 2019; Perniss et al., 2020; Rane et al., 2019; Saunders et al., 2014; Tizzano et al., 2010; Ualiyeva et al., 2020). The fact that MVCs are closely related to these cells (Fu et al., 2018; Genovese and Tizzano, 2018; Ogura et al., 2011; Ualiyeva et al., 2020) lead us to search for gene ontology enrichment related to bacterial and viral infection, immunity and inflammation for MVC_eGFP cells. We found robust enrichment of these gene ontologies in MVC_eGFP cells (Figure 3a). Transcripts related to viral infection that were higher in

MVC_eGFP cells compared to OSN_eGFP- cells (Figure 3b) included those involved in viral entry into host cells, viral transcription and regulation of viral transcription, negative regulation of viral genome replication and negative regulation of viral process (Figure 2 – figure supplement 2). The majority of these genes were detected by Ualiyeva and colleagues (Ualiyeva et al., 2020) in their ChAT-GFP MVC population. We also found gene ontology enrichment in MVC_eGFP cells compared to OSN_eGFP- cells for defense response to bacterium (Figure 2 – figure supplement 2).

Importantly, we also find enrichment for transcript expression for immunity and inflammation. Genes related to inflammation and immunity that were higher in MVC_eGFP cells compared to OSN_eGFP- cells are shown in Figure 3 – figure supplements 1-2. Among these transcripts *IL25* and its receptor *Il17rb* are enriched in MVC_eGFP cells. In SCCs, brush cells and tuft cell generation of IL25 leads to a type 2 inflammation and stimulates chemosensory cell expansion in a sequence of events that also involves cysteinyl leukotrienes (Bankova et al., 2018; Luo et al., 2019; von Moltke et al., 2016). The presence of both *Il25* and *Il17rb* suggests an autocrine effect. Furthermore, both cell types displayed increased expression of transcripts encoding for enzymes involved in eicosanoid biosynthesis such as *Alox5*, *Ptgs1* and *Ptgs2* that are found in brush cells in the airways (Bankova et al., 2018) and tuft cells in the intestine (McGinty et al., 2020) where they drive type 2 immune responses.

Transcription profiling indicates that OSN_eGFP+ cells are distinct from both OSN_eGFP- and MVC_eGFP cells. Differential gene expression analysis of the RNAseq data was used to compare OSN_eGFP+ individually with the other two groups of cells. We found that

209 expression of 2000 genes was significantly higher in OSN_eGFP+ compared to OSN_eGFP-,
210 and expression of 1821 genes was lower in OSN_eGFP+ cells (Figure 4 -figure supplement 1
211 shows the results of RNAseq and Figure 4 -figure supplement 2 summarizes the data). Figure 4
212 figure supplement 2a shows expression levels for the transcripts that showed the largest
213 differences between OSN_eGFP+ and OSN_eGFP- cells. The transcripts for TRPM5 and eGFP
214 were among the top 10 genes whose transcription was higher in OSN_eGFP+ compared to
215 OSN_eGFP- with 105-fold and 42-fold increases respectively. However all of these 10 top
216 genes, and many other genes that were found at significantly higher levels of expression in
217 OSN_eGFP+ cells compared to OSN_eGFP- happen to be genes expressed at significantly
218 higher levels in MVC_eGFP cells (Figure 4 -figure supplement 3 shows the results of RNAseq
219 for MVC_eGFP vs OSN_eGFP+). For example *Trpm5* is expressed at levels of 87.5, 9200 and
220 127000 in OSN_eGFP-, OSN_eGFP+ and MVC_eGFP cells respectively (Figure 4 -figure
221 supplement 4). While the light scatter settings in the FACS were set to exclude doublets, this
222 raised the question whether expression of these genes in the OSN_eGFP+ pool was due to
223 contamination of the OSN_eGFP+ cell fraction (mCherry and eGFP positive) by doublets made
224 up of one OSN_eGFP- cell (mCherry positive and eGFP negative) and one MVC_eGFP cell
225 (mCherry negative and GFP positive).
226
227 In order to determine whether transcription profiling for the OSN_eGFP+ cell fraction is
228 consistent with this being a separate population we searched for genes whose expression levels
229 were significantly higher in OSN_eGFP+ compared to *both* OSN_eGFP- and MVC_eGFP.
230 Figures 4a and 4b show the top genes that were expressed at significantly higher levels in
231 OSN_eGFP+ (and Figure 4 – figure supplement 5 shows data for all 80 genes). Among these

genes there were 22 olfactory receptor genes and one olfactory receptor pseudogene (Figure 4b, Figure 4c shows a volcano plot for Olfrs). A GOnet GO term enrichment analysis (Pomaznoy et al., 2018) of the 80 genes enriched in OSN_eGFP+ compared to the other two groups (Figure 4 – figure supplement 6) revealed that these cells express genes involved in sensory perception of smell (GO:0007608), signal transduction (GO:0007165) and cellular response to stimulus (GO:0051716). Interestingly, two of these genes *Trpc2* (Omura and Mombaerts, 2014) and *Calb2* (Bastianelli et al., 1995) are expressed in small subsets of OSNs. Thus, this analysis indicates that OSN_eGFP+ cells are distinct from the other two cell populations, although more detailed follow-up experiments are necessary to fully characterize this population including single cell RNA sequencing.

Gender differences for expression of olfactory receptors. We did not find major differences in transcriptome profiling between males and females for genes that were differentially expressed between the three cell groups (Figure 4 – figure supplement 7,8). We found a substantial number of olfactory receptor genes that were differentially expressed between males and females (Figure 4 – figure supplement 8). Interestingly, *Trpc2*, that is one of the genes with higher expression in OSN_eGFP+ cells is expressed in higher amounts in females. Surprisingly, the differentially expressed olfactory receptors differed from receptors identified by van der Linden et al. (van der Linden et al., 2018).

***In situ* hybridization chain reaction finds strong TRPM5 mRNA expression in MVC_eGFP cells, but not in the nuclear OSN layer.** Studies with regular *in situ* hybridization find expression of TRPM5 mRNA in MVCs, but not in the OSN nuclear layer (Pyrski et al., 2017;

Yamaguchi et al., 2014). Here we asked whether third generation in situ hybridization chain reaction version 3.0 (HCR v3.0) designed to provide high signal to noise ratio *in situ* signal (Choi et al., 2018) revealed TRPM5 mRNA expression in the nuclear OSN layer. These experiments were performed in TRPM5-GFP mice and in TRPM5-GFP mice crossed with TRPM5 knockouts (Clapp et al., 2006; Damak et al., 2006). Consistent with published results (Pyrski et al., 2017; Yamaguchi et al., 2014) we find strong *in situ* signal for TRPM5 in MVC_eGFP cells located in the apical layer of the olfactory epithelium (Figure 5a, asterisks, also see Figure 5 – figure supplement 1 for a 3D rendering) and this signal is absent in MVC_eGFP cells in the TRPM5 knockout (Figure 5b, asterisks). In addition, we find sparse TRPM5 *in situ* labeling in the nuclear OSN layer (Figure 5a, arrows), but similar sparse labeling was found in the OSN nuclear layer in the TRPM5 knockout (Figure 5b, arrows). Therefore, we find evidence for strong expression of TRPM5 mRNA in MVC_eGFP cells, but we do not find evidence for expression of TRPM5 mRNA in OSNs.

Discussion

We performed transcriptional profiling of three chemosensory cells in the mouse olfactory epithelium: microvillous cells (MVC_eGFP) and two types of olfactory sensory neurons: OSN_eGFP+ and OSN_eGFP-. We found that while the transcriptome of each of these cell types is distinct they share common features across groups. The two groups of OSNs share transcript expression for proteins expressed in OSNs such as OMP, olfactory transduction proteins, and proteins involved in synaptic function. Yet, they differ in olfactory receptor expression and OSN_eGFP+ express transcripts encoding for proteins involved in chemosensory signal transduction and cellular response to stimulus. On the other hand, MVC_eGFP cells express transcripts encoding for taste transduction proteins and other transcripts found in SCCs such as *Pou2f3* and *Il25* but they do not express transcripts for proteins involved in olfactory transduction and synaptic function, and they do not express olfactory receptors. Finally, we found that MVC_eGFP cells express a substantial number of transcripts involved in viral infection, inflammation and immunity.

Transcriptional profiling reveals a role of microvillous cells in viral infection and innate immunity. Gene ontology analysis revealed that MVC_eGFP cells are enriched in viral-related transcripts compared to OSN_eGFP- (Figure 3 and Figure 2 – figure supplement 2). GOnet GO term enrichment analysis (Pomaznoy et al., 2018) of all 133 immune genes enriched in MVC_eGFP cells compared to OSN_eGFP- (Figure 3 – figure supplement 2) revealed that MVCs express a substantial number of genes involved in the innate immune response (GO:0045087, 72 genes matched this list). Figure 6 depicts several mechanisms that could occur in MVC_eGFP in response to viral infection. To infect cells, viruses must interact with host cell

membranes to trigger membrane fusion and viral entry. Membrane proteins at the surface of the host cell are thus key elements promoting or preventing viral infection. Here we find that transcripts for several membrane proteins and cell adhesion molecules involved in viral entry are enriched in MVC_eGFP cells. *Plscr1* encodes a phospholipid scramblase which has been shown to promote herpes simplex virus (HSV) entry in human cervical or vaginal epithelial cells and keratinocytes (Cheshenko et al., 2018), and hepatitis C virus entry into hepatocytes (Gong et al., 2011). In contrast with its role in viral entry, PLSCR1 impairs the replication of other types of viruses in infected cells (influenza A virus (Luo et al., 2018), hepatitis B virus (Yang et al., 2012)). IFTM2 is another transmembrane protein that mediates viral entry. In contrast with PLSCR1, IFTM2 inhibits viral entry of human immunodeficiency virus (HIV, (Yu et al., 2015)), hepatitis C virus (Narayana et al., 2015), influenza A H1N1 virus, West Nile virus, and dengue virus (Brass et al., 2009). IFTM2 also inhibits viral replication (Brass et al., 2009) and protein synthesis (Lee et al., 2018). Nectins are transmembrane glycoproteins and constitute cell surface receptors for numerous viruses. There is wide evidence that HSV can enter host cells through Nectin-1 dependent mechanisms, particularly for neuronal entry (Kopp et al., 2009; Petermann et al., 2015; Sayers and Elliott, 2016; Shukla et al., 2012), and Nectin-4 appears essential for measles virus epithelial entry (Noyce and Richardson, 2012; Singh et al., 2015; Singh et al., 2016). In addition to cell surface molecules, the mucus contains secreted proteins that confer protection against viruses to the underlying cells. Glycoproteins are major constituents of mucus and exhibit multiple pathogens binding-sites. We found the *Ltf* transcript in MVC_eGFP cells, which encodes for lactotransferrin. Lactotransferrin is a globular glycoprotein widely represented in the nasal mucus with anti-viral activity against Epstein-Barr virus (Zheng et al., 2014; Zheng et al., 2012), HSV (Shestakov et al., 2012; Valimaa et al., 2009)) and Hepatitis C virus (Allaire et

al., 2015). Finally, MVC_eGFP cells express the murine norovirus (MNoV) receptor CD300LF. In the gut TRPM5-expressing tuft cells express high levels of CD300LF and mice were resistant to infection with $MNoV^{CR6}$ when tuft cells were absent or decreased, whereas viral titers were enhanced in any context where tuft cell numbers were increased, such as helminth infection or treatment with rIL-25 (Wilen et al., 2018).

Viruses have developed numerous strategies to overcome barrier mechanisms to enter the cells. After viral entry infected cells have other resources to fight against viral infection by disrupting the production of new viral particles, limiting inflammation processes and activating innate immune responses. For example, TRIM25, whose transcript is increased in MVC_eGFP cells, is an ubiquitin ligase that activates retinoic acid-inducible gene I (RIG-I) to promote the antiviral interferon response (Gack et al., 2007). Furthermore, influenza A virus targets TRIM25 to evade recognition by the host cell (Gack et al., 2009). In addition, TRIM25 displays a nuclear role in restricting influenza A virus replication (Meyerson et al., 2017). Zc3h12a, also known as MCPIP-1, inhibits hepatitis B and C virus replication, reduces virus-induced inflammation (Li et al., 2020; Lin et al., 2014), and exerts antiviral effects against influenza A virus (Dong et al., 2017).

We show that MVC_eGFP express *Gnat3*, *Plcg2* and *Itpr3*. This intracellular pathway would lead to calcium increase and opening of TRPM5, leading to a sodium influx and potential vesicle release. Among the list of inflammation genes enriched in MVC_eGFP we find *Il25*, an interleukin that is involved in the type 2 inflammatory response of TRPM5-expressing epithelial cells in the airway epithelium and the gut (O'Leary et al., 2019; Ting and von Moltke, 2019).

Also, *Il25* expression in the skin leads to disruption of the epithelium and enhances HSV-1 and vaccinia virus replication (Kim et al., 2013). MVC_eGFP cells are known to produce acetylcholine, which can activate sustentacular cells through M3 muscarinic acetylcholine receptors (Ogura et al., 2011). Sustentacular cells may in particular play a role in maintaining extracellular ionic gradients, extracellular glucose, secreting mucus, metabolizing noxious chemicals, and regulating cell turnover (Fu et al., 2018; Villar et al., 2017). In addition to *Il-25*, the expression of enzymes for eicosanoid biosynthesis (*Alox5*, *Ptgs1* and *Ptgs2*) suggests that MVC_eGFP are likely to recruit group 2 innate lymphoid cells, similar to tuft cells in the small intestine (McGinty et al., 2020). Finally, the innate immune response involves recruitment of macrophages that are known to play a protective role in the olfactory epithelium (Borders et al., 2007). MVC_eGFP express the G-protein coupled receptor GPR126/ADGRG6, which is required for macrophage recruitment and Schwann cells regeneration after peripheral nerve injury (Mogha et al., 2016). This raises the question whether MVC_eGFP could play a protective role, promoting OSN survival and increasing neurogenesis, through macrophage recruitment. In addition, activation of MVCs by irritants, bacteria and viruses could result in activation of cytokine-induced inflammation and macrophage recruitment by long-term horizontal basal cells, that activate type 1 immune responses within the olfactory epithelium (Chen et al., 2019). All cytokines and interferons produced in the microenvironment of a MVC_eGFP can then contribute to the activation of immune responses in neighboring MVC_eGFP, since we found the expression of various cytokine receptors (*IL6ra, Il1rap, IL4ra, IL17re, IL17 rb, TNFRSF13B*) and interferons responsive elements (*Ifitms*) .

Our findings of expression of virally relevant transcripts in MVC_eGFP cells complement published studies on the role of MVC-related SCCs in viral infection. In the trachea, viral-associated formyl peptides activate SCCs to release acetylcholine and activate mucocilliary clearance by ciliated cells (Perniss et al., 2020). This activation is mediated by the TRPM5 transduction pathway in the SCC and muscarinic acetylcholine receptors in the ciliated cell. In a similar manner in the olfactory epithelium MVCs respond to ATP, which is involved in activating mucociliary movement by releasing acetylcholine and activating adjacent sustentacular cells through a muscarinic receptor (Fu et al., 2018). Therefore, viral infection could result in activation of MVCs resulting in activation of mucociliary clearance by adjacent sustentacular cells.

Pou2f3 also called *Skn1a*, encodes for a key regulator for the generation of TRPM5-expressing cells in various epithelial tissues (Yamashita et al., 2017). *Pou2f3* transcript was increased in MVC_eGFP cells compared to OSN_eGFP-. *Skn1a/Pou2f3*-deficient mice lack intestinal tuft cells and have defective mucosal type 2 responses to helminth infection in the intestine (Gerbe et al., 2016). MVCs express markers of tuft cells (*Pou2f3*, *Trpm5* and others) indicating that MVCs share inflammatory and innate immune functions with tuft cells in the gut and SCCs and brush cells in the airways (Ting and von Moltke, 2019). In addition, in the anterior olfactory epithelium, where there is a higher density of MVCs, mice exposed to mild odorous irritants exhibited a time-dependent increase in apoptosis and a loss of mature OSNs without a significant increase in proliferation or neurogenesis (Lemons et al., 2020). Future experiments are necessary to determine whether activation of MVCs by viruses could lead to loss of mature OSNs contributing to smell loss after viral infection. Interestingly, in the mouse distal lung, where there

389 is no expression of SCCs, there was de novo generation of SCCs after infection with
390 A/H1N1/PR/8 influenza virus (Rane et al., 2019) raising the question whether virus exposure
391 could alter MVC number in the olfactory epithelium. Finally, in teleost fish rhabdoviruses induce
392 apoptosis in a unique type of crypt OSN via the interaction of the OSN TrkA receptor with the
393 viral glycoprotein and activates proinflammatory responses in the olfactory organ (Sepahi et al.,
394 2019).
395
396 **Viral infection of the central nervous system through the olfactory epithelium.** The olfactory
397 epithelium provides direct viral access to the brain through the olfactory nerve. Whether this
398 olfactory path constitutes route of entry for viruses to the brain is a matter of intense discussion,
399 especially because some viruses are postulated to be involved in encephalopathy and
400 neurodegenerative disorders (Cairns et al., 2020; Dando et al., 2014; Doty, 2008; Harris and
401 Harris, 2018). Our finding that MVC_eGFP cells are enriched in virally-related genes suggests
402 that these cells may be involved in or prevention of viral entry into the brain (and these two
403 alternatives are not exclusive since they may be different for different viruses). On the one hand,
404 we identified transcripts encoding for viral receptors in MVC_eGFP, suggesting that viruses can
405 enter these cells. It is not known whether viruses can spread in neighboring cells, but if viral
406 particles were to enter the OSNs they could reach the olfactory bulb through anterograde
407 transport along the olfactory nerve and from the olfactory bulb, viruses can spread throughout
408 the brain along the olfactory bulb-hippocampus route. On the other hand, we found enrichment
409 for transcripts encoding for proteins involved in limiting viral infection and promoting immune
410 and anti-inflammatory responses in MVC_eGFP cells. In this case, viral spread to the brain
411 would be prevented. Finally, the olfactory epithelium is innervated by the trigeminal nerve, and

substance P immunostaining is closely associated with subsets of MVCs (Lin et al., 2008). This raises the question whether an interaction between MVCs and trigeminal nerve fibers could participate in local inflammation as found for SCCs (Saunders et al., 2014), and could modulate the entry of virus to the brain stem through the trigeminal nerve. Future experiments are necessary to study the potential role of MVC_eGFP cells in viral infection of the olfactory epithelium and the brain.

Are GFP-expressing OSNs in the TRPM5-GFP mouse a distinct set of OSNs? Expression of TRPM5 in a subset of OSNs has been controversial. The original proposal of expression of TRPM5 in OSNs was motivated by expression of eGFP in adult TRPM5-eGFP transgenic mice and immunolabeling of the ciliary layer of the epithelium with an antibody (raised against the TRPM5 peptide RKEAQHKRQHLERDLPDPLDQK) that was validated by lack of expression in TRPM5 knockout mice(Lin et al., 2007). However, staining in the ciliary layer with this antibody has not been replicated and our group and others subsequently showed knockout-validated TRPM5 staining of microvillous cells, and no labeling of the ciliary layer in the adult with antibodies raised against different TRPM5 protein peptides(Genovese and Tizzano, 2018; Gilbert et al., 2015; Lin et al., 2008; Pyrski et al., 2017). Interestingly, Pyrski and co-workers found TRPM5 immunolabeling in OSNs in the embryo, but not in the adult(Pyrski et al., 2017). Furthermore, in the adult mouse *in situ* hybridization has reported mRNA staining for TRPM5 in MVCs, and not in OSNs(Pyrski et al., 2017; Yamaguchi et al., 2014), and full length TRPM5 mRNA was not found in OSNs in the adult(Pyrski et al., 2017).

Here we corroborate expression of eGFP in OSNs in TRPM5-eGFP transgenic mice. In addition, using HCR v3.0 we find strong expression of mRNA in MVCs, but we do not find evidence for expression of TRPM5 mRNA in OSNs (Figure 5). However, transcriptional analysis indicates that the OSN_eGFP+ cell population differs in mRNA expression from the other two populations (Figure 4). OSN_eGFP+ express a subset of olfactory receptors as well as transcripts encoding for proteins involved in chemosensory signal transduction and cellular response to stimulus. This is consistent with calcium imaging and loose patch recordings from adult TRPM5-eGFP transgenic mice that found that GFP-labeled cells with morphology resembling OSNs (presumably OSN_eGFP+ cells) responded to pheromones and MHC peptides with currents that were abolished by pharmacologic inhibition of TRPM5 or isolation of cells from TRPM5 knockouts(Lopez et al., 2014). In addition, studies of neuronal connectivity found that approximately half of the glomeruli innervated by GFP-bearing axons in the adult TRPM5-eGFP transgenic mouse are innervated by mitral cells that project directly to the medial amygdala, consistent with these glomeruli carrying pheromone information(Thompson et al., 2012). Nevertheless, these findings are in contrast with findings by Pyrksi and co-workers who show that in adult Trpm5-IRES-Cre x R26-GCaMP3 mouse OSNs that express GCaMP3 do not respond selectively to pheromones, and responded to general odorants(Pyrski et al., 2017). Why the functional studies of Lopez and co-workers and Pyrski and co-workers differ is not clear. However, eGFP-bearing OSNs in the Trpm5-IRES-Cre crossed with an eGFP reporter were expressed throughout the olfactory epithelium with no obvious spatial pattern (Pyrski et al., 2017) in contrast with the expression of eGFP in TRPM5-eGFP transgenics that is stronger in the lateral olfactory epithelium(Oshimoto et al., 2013). This raises the question whether eGFP is expressed in different OSNs in the Trpm5-IRES-Cre and TRPM5-eGFP transgenics. In

summary, our data indicate that OSN_eGFP+ cells are a distinct population of chemosensory cells, but whether these are pheromone-responding OSNs requires future studies.

Would microvillous cells play a role in COVID-19? Recently, due to the current COVID-19 pandemic, researchers have focused their attention on investigating SARS-CoV-2 mechanism of entry into cells. SARS-CoV-2 targets mainly cells of the respiratory pathway where viral entry is mediated by ACE2 and TMPRSS2 (Hoffmann et al., 2020). Because numerous patients reported loss of smell (Giacomelli et al., 2020; Parma et al., 2020; Yan et al., 2020a; Yan et al., 2020b), researchers wondered about the mechanism for SARS-CoV-2 infection of the olfactory epithelium. In our study, we found the *Tmprss2* transcript was significantly increased in MVC_eGFP cells compared to OSN_eGFP- (Figure 3). We did not find *Ace2* enrichment in these cells, but this may be due to inefficiency in finding with RNAseq low abundance transcripts like *Ace2* (Ziegler et al., 2020). Transcriptional profiling of single cells in the olfactory epithelium from other laboratories found expression of transcripts for both *Tmprss2* and *Ace2* in in sustentacular cells and stem cells, and at lower levels in MVCs (Brann et al., 2020; Fodoulian et al., 2020). Viral infection of sustentacular cells may explain loss of smell because these cells play a key role in supporting olfactory function by providing glucose for the energy necessary for olfactory transduction in the OSN cilia (Villar et al., 2017). Importantly, type I interferons, and to a lesser extent type II interferons induced by response of the host to SARS-CoV-2, and infection by other viruses inducing the interferon pathway increases *Ace2* expression in the nasal epithelium (Ziegler et al., 2020). MVCs may play a role in SARS-CoV-2 infection of the olfactory epithelium because these cells may participate in activating inflammation of the epithelium that elicits type 1 immune response (Chen et al., 2019).

Conclusion. Here we find that microvillous cells of the olfactory epithelium express transcripts involved in immunity, inflammation and viral infection. These expression patterns suggest that, like tuft cells in the gut and SCCs and brush cells in the airways, the microvillous cells in the olfactory epithelium are involved in the innate immune response to viral infection. Our study provides new insights into a potential role for TRPM5-expressing cells in viral infection of the main olfactory epithelium.

Abbreviations

COVID-19: Coronavirus disease 2019

DPI: Days post infection

eGFP: Enhanced green fluorescent protein

FACS: Fluorescence-activated cell sorting

FDR: False discovery rate

GLM: Generalized linear model

GO: Gene ontology

MVCs: Microvillous cells

OMP: Olfactory marker protein

OSNs: Olfactory sensory neurons

PSF: Point spread function

SARS-CoV-2: Severe acute respiratory syndrome coronavirus clade 2

SSC: Saline-sodium citrate

SSCT: SSC with tween

TRPM5: Transient receptor potential cation channel subfamily M member 5

Methods

Key Resources Table

REAGENT TYPE	REAGENT or RESOURCE	SOURCE	IDENTIFIER	ADDITIONAL INFORMATION
Chemical compound, drug	BrainPhys Neuronal Medium	Stemcell Technologies		Product # 05791
Chemical compound, drug	Dispase II	Sigma		Product # D4693
Chemical compound, drug	AcGFP1/eGFP calibration beads	Takara		Flow cytometry calibration beads Product # 632594
Chemical compound, drug	mCherry calibration beads	Takara		Flow cytometry calibration beads Product # 632595
Chemical compound, drug	RQ1 RNase-free DNase	Promega		Product # M6101
Chemical compound, drug	Papain	Sigma		Product # P3125
Chemical compound, drug	Paraformaldehyde (32%)	Electron Microscopy Sciences		Product # 157145
Chemical compound, drug	RNAprotect Tissue Reagent	Qiagen		Product # 76526
Chemical compound, drug	RNeasy Plus Micro Kit	Qiagen		Product # 74034
Chemical compound, drug	High Capacity c-DNA Reverse Transcription kit	ABI		
Chemical compound, drug	18s rRNA	PE ABI		
Strain, strain background	TRPM5-eGFP	Dr. Robert Margolskee (Clapp et al., 2006)		
Strain, strain background	TRPM5 knockout	Dr. Robert Margolskee {Damak, 2006 #1567}		
Strain, strain background	OMP-H2B::Cherry	Generated for this publication		This mouse will be deposited in Jackson Laboratories
Software, algorithm	MATLAB_R2018a	Mathworks	RRID: SCR_001622	

Software, algorithm	Illustrator	Adobe	RRID: SCR_010279	
Software, algorithm	Photoshop	Adobe	RRID: SCR_014199	
Software, algorithm	InDesign	Adobe		
Software, algorithm	MoFlo Astrios Summit Software (6.3.1.16945).	Beckman Coulter		
Software, algorithm	BBMap (BBDuk)		RRID:SCR_016968	
Software, algorithm	Salmon v1.2.1	https://combine-lab.github.io/salmon/	RRID:SCR_017036	(Patro et al., 2017)
Software, algorithm	DeSEQ2 v1.28.0	bioconductor.org https://bioconductor.org/packages/release/bioc/html/DESeq2.html	RRID:SCR_015687	(Love et al., 2014)
Software, algorithm	TopGO, v2.40.0		RRID:SCR_014798	
Software, algorithm	pHeatmap, 1.0.12		RRID:SCR_016418	
Software, algorithm	Ensembl GRCm38, v99			
Software, algorithm	R, v4.0		RRID:SCR_001905	
Software, algorithm	Tximport, v1.16.0		RRID:SCR_016752	
Software, algorithm	SAMtools	SAMtools http://samtools.sourceforge.net/	RRID:SCR_002105	(Li et al., 2009)
Software, algorithm	Bedtools		RRID:SCR_006646	
Software, algorithm	STAR v2.5.3a	https://github.com/alexdobin/STAR	RRID:SCR_015899	
Software, algorithm	Sigmaplot, v12.5	Systat Software	RRID:SCR_003210	
Software, algorithm	Custom code for bioinformatics analysis	https://github.com/eric-d-larson/OE_TRPM5		
Software, algorithm	OPM	https://github.com/qi2lab/opm		

506

Overview of the method for transcriptional profiling of low abundance cell populations. For transcriptional profiling of TRPM5-bearing MVC_eGFP cells and OSN_eGFP+ cells that constitute a small fraction of the cells in the epithelium, we used FACS to separate the cell populations targeted for RNAseq (Amamoto et al., 2019). In our experiments, we isolated the cells from mice that expressed fluorescent marker proteins appropriate for cell sorting. OSNs were expressing mCherry under the control of OMP promoter. eGFP was expressed in MVCs and a subset of OSNs (OSN_eGFP+ cells) under control of the TRPM5 promoter.

Generation of OMP-H2B::Cherry mice. A PacI cassette containing PacI-H2B::mCherry-pA PGK-puro-pA-PacI was inserted into an OMP gene-targeting vector (pPM9)(Mombaerts et al., 1996), which replaces the OMP coding sequence with the PacI cassette and expresses a H2B::mCherry fusion protein. Animals are maintained in a mixed 129/B6 background.

Animals. Mice with TRPM5-driven eGFP expression (Clapp et al.,2006) were crossed with OMP-H2B::Cherry mice. The TRPM5-eGFP mice and TRPM5 knockout mice(Damak et al., 2006) were obtained with written informed consent from Dr. Robert Margolskee. Lines were maintained separately as homozygous and backcrossed regularly. Experiments were performed on mice from the F1 generation cross of TRPM5-eGFP and OMP-H2B::Cherry mice (OMP-H2B::mCherry/TRPM5-eGFP). PCR was used to verify genotype of experimental mice for eGFP and mCherry expression. Both male and female mice were used for experiments with ages ranging from 3- 8 months. Estrous and cage mate information was collected for all female mice in conjunction with experimental use. Mice were housed in passive air exchange caging under a 12:12 light/dark cycle and were given food and water *ad libitum*. Mice were housed in the

National Institutes of Health approved Center for Comparative Medicine at the University of Colorado Anschutz Medical Campus. All procedures were performed in compliance with University of Colorado Anschutz Medical Campus Institutional Animal Care and Use Committee (IACUC) that reviews the ethics of animal use.

In our vivarium we have ventilated cages (HV cages) where air is mechanically exchanged with fresh air once every minute and static cages (LV cages) where air is exchanged passively through a filter in the cover. When we moved the OMP-H2B::mCherry/TRPM5-eGFP to HV cages we noticed a decrease in the number of OSN_eGFP+ cells sorted per mouse (Figure 1-figure supplement 1a,b and c), suggesting that changes in ventilation conditions affect TRPM5 promoter-driven expression of eGFP. Following this observation, mice were moved back to LV cages. We proceeded to study the dependence of the number of OSN_eGFP+ cells sorted on the number of days in LV vs. HV cages. The number of OSN_eGFP+ cells is positively correlated with the number of days the animal spends in LV cages (Figure 1 – figure supplement 1d) and negatively correlated to the number of days the animals spend in the HV cages (Figure 1 – figure supplement 1e). Generalized linear model (GLM) analysis found significant differences for the number of OSN_eGFP+ cells sorted as a function of the number of days in LV cages ($p<0.05$, 26 observations, 24 d.f., F-statistic = 5.64, p-value for GLM <0.05) and the number of days in HV cages ($p<0.05$, 26 observations, 24 d.f., F-statistic = 5.99, p-value for GLM <0.05). For RNAseq experiments one FACS sort was done using cells from mice born and maintained in HV housing, and the OSN_eGFP+ yield was low. Subsequently, we performed all FACS with cells isolated from the olfactory epithelium of mice raised in LV cages.

553 **Tissue dissociation of the olfactory epithelium.** Following euthanasia via CO2 inhalation, the
554 olfactory epithelium was immediately removed from the nasal cavity and epithelial tissue was
555 separated from the bone in the turbinates. Care was taken not to include respiratory epithelium.
556 The epithelium was dissociated enzymatically with Dispase II (2 mg/ml) diluted in Ringer's
557 solution (145mM NaCl, 5mM KCL, 20mM HEPES, 1mM $MgCL_2$, 1mM $CaCl_2$, 1mM Ny-
558 Pyruvate, 5mM Glucose) (~25 minutes at 37^0C) followed by an incubation in a papain plus
559 Ca/Mg++ free Ringer's solution (Ca/Mg++ free Ringer's: 145mM NaCl, 5mM KCL, 20mM
560 HEPES, 1mM Ny-Pyruvate, 1mM EDTA , L-cysteine: 1mg L-cysteine /1.5mL Ca/Mg++ free
561 Ringer's, Papain:1-3ul/1mL Ca/Mg++ free Ringer's), for ~40-45 minutes at 37^0C. Following
562 incubation, DNase I (Promega) at 0.05U/µl and RNAse free 10x Reaction buffer (1:20) were
563 added to solution and the tissue was gently triturated using a ~1mm opening pipette. Isolated
564 OSNs were collected from supernatants via centrifugation and resuspended in cell sorting
565 medium of 1x PBS (diluted from commercial 10x PBS, pH 7.4) and BrainPhys Neuronal
566 Medium (Stemcell Technologies). Initially, isolated cells were examined with a confocal
567 microscope to confirm efficacy of dissociation methods, and examine cell types and
568 fluorescence. For RNAseq, cells were strained through a 40 µm cell strainer and kept on ice until
569 sorted via flow cytometry.
570
571 **Flow cytometry.** Fluorescence activated cell sorting was performed in the University of
572 Colorado Cancer Center Flow Cytometry Core on a Beckman Coulter MoFlo Astrios EQ using
573 MoFlo Astrios Summit Software (6.3.1.16945). eGFP signal was detected using a 488 nm laser
574 and a bandpass 526/52nm collection filter. mCherry signal was detected using a 561 nm laser
575 and a bandpass 614/20 nm collection filter. The 488nm laser was also used to detect light

scatter. The threshold was set at 3%. Gating was set to exclude doublets and optimized as cell populations emerged based on fluorescent markers. Flow cytometry calibration beads for AcGFP1/eGFP and mCherry (Takara, 632594, 632595) were used as fluorescence intensity controls. Olfactory epithelium cell suspensions from wild type and OMP-H2B::Cherry mice or TRPM5-eGFP mice were sorted as controls for auto fluorescence for eGFP and mCherry populations respectively. Cells were sorted into RNAprotect Tissue Reagent (Qiagen).

RNA-extraction. Total RNA was extracted from sorted, pooled cells from each cell population using the RNeasy Plus Micro Kit (Qiagen) according to the manufacturers recommended protocol.

RT-qPCR. Quantitative reverse transcription polymerase chain reaction (RT-qPCR) was used to assess and confirm identities of cell types from each of the sorted cell populations. Following total RNA extraction, RT-qPCR was performed in the PCR core at University of Colorado Anschutz Medical Campus for the following markers: OMP, TRPM5, eGFP and ChAT. Primers and probes used for eGFP, TRPM5 and OMP were described in (Oshimoto et al., 2013). Predesigned primers and probes for ChAT were purchased from Life Technologies. The mRNA for these targets was measured by RT-qPCR using ABI QuantStudio 7 flex Sequence detector. 1µg total RNA was used to synthesize cDNA using the High Capacity c-DNA Reverse Transcription kit (ABI-P/N 4368814). cDNA was diluted 1: 2 before PCR amplification.

The TaqMan probes were 5'labeled with 6-carboxyfluorescein (FAM). Real time PCR reactions were carried out in MicroAmp optical tubes (PE ABI) in a 25 µl mix containing 8 % glycerol,

1X TaqMan buffer A (500 mM KCl, 100 mM Tris-HCl, 0.1 M EDTA, 600 nM passive reference dye ROX, pH 8.3 at room temperature), 300 µM each of dATP, dGTP, dCTP and 600 µM dUTP, 5.5 mM MgCl2, 1X primer-probe mix, 1.25 U AmpliTaq Gold DNA and 5 µl template cDNA. Thermal cycling conditions were as follows: Initiation was performed at 50^{o}C for 2 min followed by activation of TaqGold at 95^{o}C for 10 min. Subsequently 40 cycles of amplification were performed at 95^{o}C for 15 secs and 60^{o}C for 1 min. Experiments were performed with duplicates for each data point. Each PCR run included the standard curve (10 fold serially diluted pooled cDNA from control and experimental samples), test samples, no-template and NORT controls. The standard curve was then used to calculate the relative amounts of targets in test samples. Quantities of targets in test samples were normalized to the corresponding 18s rRNA (PE ABI, P/N 4308310).

RNA sequencing and pre-processing. RNA quality control, library preparation, and sequencing were performed at the University of Colorado Genomics and Microarray core. Extracted RNA was used as the input for the Nugen Universal Plus mRNA-seq kit (Redwood City, CA) to build stranded sequencing libraries. Indexed libraries were sequenced using an Illumina NovaSEQ6000. Library preparation and sequencing was performed in two batches, separated by gender. 11 female samples were sequenced with an average depth of 37.3 million +/- SD of 6.5 million read pairs, and 25 male samples were sequenced with an average depth of 34.8 million +/- SD of 3.5 million read pairs. Metadata for the samples submitted are shown in Figure 2 - figure supplement 3. Raw BCL files were demultiplexed and converted to FASTQ format. Trimming, filtering, and adapter contamination removal was performed using BBDuk (Bushnell).

RNA Sequencing Analysis. Transcript abundance was quantified from trimmed and filtered FASTQ files using Salmon v1.2.1(Patro et al., 2017) and a customized Ensembl GRCm38 (release 99) transcriptome (Zerbino et al., 2018). A customized version of the transcriptome was prepared by appending FASTA sequences of eGFP and mCherry to the GRCm38 FASTA file. The corresponding gene transfer format (GTF) file was modified accordingly to incorporate the new transcripts. Transcript abundance was summarized at the gene level using the TxImport (Soneson et al., 2015) package in R. Differential gene expression was quantified using DESeq2 (Love et al., 2014) with default parameters after removing genes with an average count of < 5 reads in each group. Significance was determined by FDR-adjusted p-value < 0.05. TopGO was used for gene ontology analysis (Alexa and Rahnenfuhrer, 2020). The input to TopGO was a list of significant DEGs and a list of all detected genes in the dataset. Enrichment was calculated by dividing the number of detected genes by the number of expected genes within each ontology of the TopGO output. To make the bar graphs in Figures 4 and 5, enrichment scores of downregulated GO terms were multiplied by -1 for visualization. Heatmap visualization was performed using *pHeatmap* in R (Kolde, 2019).

RNA-sequence data comparison with Ualiyeva et al 2020

Raw counts for this study and for Ualiyeva et al (GEO GSE139014)(Ualiyeva et al., 2020) were converted to log10(reads per million (RPM) +1). These RPM values were used to generate heatmaps to show the expression values of specific transcripts. No quantitative assessment was performed between the two studies.

645

646 **Tissue Preparation for Fluorescence Microscopy and *in situ*.** For euthanasia, mice were
647 anesthetized with ketamine/xylazine (20–100 _g/g of body weight), perfused transcardially with
648 0.1 M phosphate buffer (PBS) followed by a PBS-buffered fixative (EMS 32%
649 Paraformaldehyde aqueous solution diluted to 4% with 1x PBS) . The nose was harvested and
650 postfixed for 12 h before being transferred for cryoprotection into PBS with 20% sucrose
651 overnight. The olfactory epithelium was cryosectioned coronally into 16 µm -thick sections
652 mounted on Superfrost Plus slides (VWR, West Chester, PA) coated with poly-D-lysine.

653

654 ***In situ* followed by immunohistochemistry (IHC).** *In situ* hybridization was performed with
655 the hybridization chain reaction method (Choi et al., 2018) using HCR v3.0 Probe Sets,
656 Amplifiers, and Buffers from Molecular Instruments, Inc. Frozen slides were allowed to thaw
657 and dry, baked at 60°C for 1 hour, then immersed in 70% ethanol overnight at 4°C, and allowed
658 to dry again completely. Slides were inverted and placed on a Plexiglas platform inside a
659 humidified chamber; subsequent steps were performed using this setup. Slides were incubated in
660 10 µg/µl proteinase K for 15 minutes at 37°C, then pre-hybridized with HCR hybridization
661 buffer (30% formamide buffer from Molecular Instruments) for 30 minutes at 37°C. *Trpm5-B3*
662 probes and *OMP-B2* probes (0.8 pmol of each probe in 100 µl HCR hybridization buffer per
663 slide) were added, and slides were hybridized overnight at 37°C. Slides were briefly incubated in
664 undiluted HCR Wash Buffer (30% formamide buffer from Molecular Instruments) for 20
665 minutes at 37°C. Excess probes were removed by incubating slides for 20 minutes each at 37°C
666 in solutions of 75% HCR Wash Buffer / 25% SSCT (5X SSC, 0.1% Tween, diluted in RNAse
667 free water), 50% Buffer / 50% SSCT, 25% Buffer / 75% SSCT, and 100% SSCT. Slides were

incubated in 100% SSCT at room temperature for 20 minutes, then in Amplification Buffer (Molecular Instruments) at room temperature for 1 hour. B3 hairpins labeled with Alexa Fluor 647 and B2 hairpins labeled with Alexa Fluor 546 were prepared (12 pmol of each hairpin were heat shocked, then cooled for 30 minutes, and added to 200µl of Amplification Buffer) added to slides, and incubated overnight at room temperature. Excess hairpins were removed with four washes (20 minutes) in SSCT at room temperature. Slides were then processed with IHC protocol to stain for GFP. At room temperature, tissue was permeabilized with Triton X-100 0.1% in PBS for 30 minutes, washed three times with PBS, blocked with Donkey serum 5% and Tween 20 0.3% in PBS for 1 hour, incubated with Chicken anti-GFP primary antibody (1:500 in blocking solution, AB_2307313 Aves labs) overnight, washed three times with PBS and incubated with Donkey anti-Chicken secondary antibody conjugated with alexa fluor 488 (1:500 in blocking solution, 703-545-155 Jackson ImmunoResearch laboratories).After three final washes with PBS, slides were mounted using Fluoromount-G™ mounting medium with DAPI (Thermo Fisher Scientific).

Confocal fluorescence microscopy. Microscopy was performed with confocal microscopes (Leica SP8, Nikon A1R or 3i Marianas).

Three-dimensional tissue imaging. For three-dimensional imaging, a high numerical aperture (NA) oblique plane microscope was used (Dunsby, 2008; Sapoznik et al., 2020). Briefly, this variant on a light sheet microscope only uses one objective to interface with the sample. The sample is illuminated from the epi-direction using an obliquely launched light sheet. Emitted fluorescence is detected through the same primary objective used for illumination. A secondary

and tertiary objective optically resample the emitted fluorescence to image the fluorescence resulting from the obliquely launched light sheet onto a detector(Dunsby, 2008; Sapoznik et al., 2020). For the primary, secondary, and tertiary objectives we used a high-NA silicone immersion objective (Nikon ×100 NA 1.35, 0.28–0.31 mm working distance), a high-NA air immersion objective (Nikon ×40 NA 0.95, 0.25–0.16 mm working distance), and a bespoke glass-tipped objective (AMS-AGY v1.0, NA 1.0, 0 mm working distance), respectively. Images were acquired by a high-speed scientific CMOS camera (Photometrics Prime BSI) using custom Python software ((Sapoznik et al., 2020), https://github.com/qi2lab/opm).

The obliquely launched light sheet was set to 30 degrees above the coverslip. The sample was translated in one lateral dimension (x) at a constant speed by a scan optimized stage. The scan speed was set so that images with a 5-millisecond exposure time were acquired at 200 nm spacing over a distance of 5.5 mm. This constant speed scan was performed for the same volume, cycling through three excitation wavelengths (405, 488, 635 nm) and three sample height positions (z), with 20% overlap. Once the cycle of wavelengths and height positions completed, the sample was then laterally displaced (y), again with a 20% overlap, and the scan was repeated over a 5.5 mm x 5.5 mm x .035 mm (x,y,z) imaging volume. Raw data was orthogonally deskewed, stitched, and fused using custom Python code and BigStitcher(Hörl et al., 2019). After export, each inset image was deconvolved using Microvolution and measured point spread functions.

Statistical analysis. Statistical analysis was performed in Matlab (Mathworks, USA). Statistical significance was estimated using a generalized linear model (GLM), with post-hoc tests for all data pairs corrected for multiple comparisons using false discovery rate (Curran-Everett, 2000).

The post hoc comparisons between pairs of data were performed either with a t-test, or a ranksum test, depending on the result of an Anderson-Darling test of normality. 95% CIs shown in the figures as vertical black lines or shading bounding the lines were estimated by bootstrap analysis of the mean by sampling with replacement 1000 times using the bootci function in MATLAB.

Declarations

Ethics approvals. Mouse experiments were carried out under guidelines of the National Institutes of Health in compliance with University of Colorado Anschutz Medical Campus Institutional Animal Care and Use Committee (IACUC).

Consent for publication. Not applicable.

Availability of data and materials. All data sequencing data are available in NCBI SRA https://www.ncbi.nlm.nih.gov/sra/PRJNA632936. The code used for bioinformatics analysis is found in https://github.com/eric-d-larson/OE_TRPM5

Competing interests. The authors declare no competing interests.

Funding. This work was supported by NIDCD DC014253 and NIA DC014253-04S1 (DR), by the RNA Bioscience Initiative of the University of Colorado Anschutz Medical Campus (DS and DR) and by NIDCD R21DC018864 (EDL). A Starr Stem Cell Grant (JA, AKH and PF) supported the production and characterization of the OMP-H2B::mCherry mouse strain. The funding bodies had no role in the experimental design or collection, analysis and interpretation of data or in writing the manuscript.

Authors' contributions. D.R., B.D.B., M.N. and V.R. conceptualized the project. B.D.B. performed FACS, qPCR and RNAseq experiments. E.D.L. performed genomic analysis. P.F.

745 generated the OMP-H2B::Cherry mice. D.S. designed and analyzed in situ experiments. M.N.,
746 A.N.B. and C.N. designed experiments. C.N. and J.H.Jr. performed experiments. M.L.
747 performed in situ experiments and literature search and wrote the section on viral infection in the
748 discussion. All authors contributed to writing and editing the manuscript.
749
750 ***Acknowledgements:*** We would like to acknowledge the support of Nicole Arevalo for laboratory
751 support, Jerome Artus and Anna-Katerina Hadjantonakis for the construction of the targeting
752 vector and production of OMP-H2B::Cherry mice, Emily Liman for providing TRPM5 and
753 TRPC2 antibody and Catherine Dulac for providing tissue from TRPC2 knockouts.
754

References

Alexa, A., and Rahnenfuhrer, J. (2020). topGO: Enrichment Analysis for Gene Ontology (R Package).

Allaire, A., Picard-Jean, F., and Bisaillon, M. (2015). Immunofluorescence to Monitor the Cellular Uptake of Human Lactoferrin and its Associated Antiviral Activity Against the Hepatitis C Virus. J Vis Exp, 53053.

Amamoto, R., Garcia, M.D., West, E.R., Choi, J., Lapan, S.W., Lane, E.A., Perrimon, N., and Cepko, C.L. (2019). Probe-Seq enables transcriptional profiling of specific cell types from heterogeneous tissue by RNA-based isolation. Elife *8*, e51452.

Bankova, L.G., Dwyer, D.F., Yoshimoto, E., Ualiyeva, S., McGinty, J.W., Raff, H., von Moltke, J., Kanaoka, Y., Frank Austen, K., and Barrett, N.A. (2018). The cysteinyl leukotriene 3 receptor regulates expansion of IL-25-producing airway brush cells leading to type 2 inflammation. Sci Immunol *3*, eaat9453.

Bastianelli, E., Polans, A.S., Hidaka, H., and Pochet, R. (1995). Differential distribution of six calcium-binding proteins in the rat olfactory epithelium during postnatal development and adulthood. Journal of Comparative Neurology *354*, 395-409.

771 Borders, A.S., Getchell, M.L., Etscheidt, J.T., van Rooijen, N., Cohen, D.A., and Getchell, T.V.
772 (2007). Macrophage depletion in the murine olfactory epithelium leads to increased neuronal
773 death and decreased neurogenesis. Journal of Comparative Neurology *501*, 206-218.

774 Brann, D.H., Tsukahara, T., Weinreb, C., Lipovsek, M., Van den Berge, K., Gong, B., Chance,
775 R., Macaulay, I.C., Chou, H.-J., Fletcher, R.B., *et al.* (2020). Non-neuronal expression of SARS-
776 CoV-2 entry genes in the olfactory system suggests mechanisms underlying COVID-19-
777 associated anosmia. Science Advances *6*, eabc5801.

778 Brass, A.L., Huang, I.C., Benita, Y., John, S.P., Krishnan, M.N., Feeley, E.M., Ryan, B.J.,
779 Weyer, J.L., van der Weyden, L., Fikrig, E., *et al.* (2009). The IFITM proteins mediate cellular
780 resistance to influenza A H1N1 virus, West Nile virus, and dengue virus. Cell *139*, 1243-1254.

781 Bushnell, B. BBMap (SourceForge).

782 Cairns, D.M., Rouleau, N., Parker, R.N., Walsh, K.G., Gehrke, L., and Kaplan, D.L. (2020). A
783 3D human brain–like tissue model of herpes-induced Alzheimer's disease. Science Advances *6*,
784 eaay8828.

785 Chen, M., Reed, R.R., and Lane, A.P. (2019). Chronic Inflammation Directs an Olfactory Stem
786 Cell Functional Switch from Neuroregeneration to Immune Defense. Cell Stem Cell *25*, 501-513
787 e505.

788 Cheshenko, N., Pierce, C., and Herold, B.C. (2018). Herpes simplex viruses activate
789 phospholipid scramblase to redistribute phosphatidylserines and Akt to the outer leaflet of the
790 plasma membrane and promote viral entry. PLoS Pathog *14*, e1006766.

791 Choi, H.M., Schwarzkopf, M., Fornace, M.E., Acharya, A., Artavanis, G., Stegmaier, J., Cunha,
792 A., and Pierce, N.A. (2018). Third-generation in situ hybridization chain reaction: multiplexed,
793 quantitative, sensitive, versatile, robust. Development *145*, dev165753.

794 Clapp, T.R., Medler, K.F., Damak, S., Margolskee, R.F., and Kinnamon, S.C. (2006). Mouse
795 taste cells with G protein-coupled taste receptors lack voltage-gated calcium channels and
796 SNAP-25. BMC Biol *4*, 7.

797 Curran-Everett, D. (2000). Multiple comparisons: philosophies and illustrations. AmJPhysiol
798 RegulIntegrComp Physiol *279*, R1-R8.

799 Damak, S., Rong, M., Yasumatsu, K., Kokrashvili, Z., Perez, C.A., Shigemura, N., Yoshida, R.,
800 Mosinger, B., Jr., Glendinning, J.I., Ninomiya, Y., *et al.* (2006). Trpm5 null mice respond to
801 bitter, sweet, and umami compounds. Chem Senses *31*, 253-264.

802 Damak, S., Rong, M., Yasumatsu, K., Kokrashvili, Z., Varadarajan, V., Zou, S., Jiang, P.,
803 Ninomiya, Y., and Margolskee, R.F. (2003). Detection of sweet and umami taste in the absence
804 of taste receptor T1r3. Science *301*, 850-853.

805 Dando, S.J., Mackay-Sim, A., Norton, R., Currie, B.J., St John, J.A., Ekberg, J.A.K., Batzloff,
806 M., Ulett, G.C., and Beacham, I.R. (2014). Pathogens Penetrating the Central Nervous System:
807 Infection Pathways and the Cellular and Molecular Mechanisms of Invasion. Clinical
808 Microbiology Reviews *27*, 691-726.

809 Dong, C., Sun, X., Guan, Z., Zhang, M., and Duan, M. (2017). Modulation of influenza A virus
810 replication by microRNA-9 through targeting MCPIP1. J Med Virol *89*, 41-48.

811 Doty, R.L. (2008). The olfactory vector hypothesis of neurodegenerative disease: is it viable?
812 Ann Neurol *63*, 7-15.

813 Dunsby, C. (2008). Optically sectioned imaging by oblique plane microscopy. Opt Express *16*,
814 20306-20316.

815 Farbman, A.I., and Margolis, F.L. (1980). Olfactory marker protein during ontogeny:
816 immunohistochemical localization. Developmental biology *74*, 205-215.

817 Fischl, A.M., Heron, P.M., Stromberg, A.J., and McClintock, T.S. (2014). Activity-dependent
818 genes in mouse olfactory sensory neurons. Chem Senses *39*, 439-449.

819 Fodoulian, L., Tuberosa, J., Rossier, D., Landis, B.N., Carleton, A., and Rodriguez, I. (2020).
820 SARS-CoV-2 receptor and entry genes are expressed by sustentacular cells in the human
821 olfactory neuroepithelium. bioRxiv, 2020.2003.2031.013268.

822 Fu, Z., Ogura, T., Luo, W., and Lin, W. (2018). ATP and Odor Mixture Activate TRPM5-
823 Expressing Microvillous Cells and Potentially Induce Acetylcholine Release to Enhance
824 Supporting Cell Endocytosis in Mouse Main Olfactory Epithelium. Front Cell Neurosci *12*, 71.

825 Gack, M.U., Albrecht, R.A., Urano, T., Inn, K.S., Huang, I.C., Carnero, E., Farzan, M., Inoue,
826 S., Jung, J.U., and Garcia-Sastre, A. (2009). Influenza A virus NS1 targets the ubiquitin ligase
827 TRIM25 to evade recognition by the host viral RNA sensor RIG-I. Cell Host Microbe *5*, 439-
828 449.

829 Gack, M.U., Shin, Y.C., Joo, C.H., Urano, T., Liang, C., Sun, L., Takeuchi, O., Akira, S., Chen,
830 Z., Inoue, S., *et al.* (2007). TRIM25 RING-finger E3 ubiquitin ligase is essential for RIG-I-
831 mediated antiviral activity. Nature *446*, 916-920.

832 Genovese, F., and Tizzano, M. (2018). Microvillous cells in the olfactory epithelium express
833 elements of the solitary chemosensory cell transduction signaling cascade. PLoS One *13*,
834 e0202754.

835 Gerbe, F., Sidot, E., Smyth, D.J., Ohmoto, M., Matsumoto, I., Dardalhon, V., Cesses, P.,
836 Garnier, L., Pouzolles, M., Brulin, B., *et al.* (2016). Intestinal epithelial tuft cells initiate type 2
837 mucosal immunity to helminth parasites. Nature *529*, 226-230.

838 Giacomelli, A., Pezzati, L., Conti, F., Bernacchia, D., Siano, M., Oreni, L., Rusconi, S.,
839 Gervasoni, C., Ridolfo, A.L., Rizzardini, G., *et al.* (2020). Self-reported olfactory and taste
840 disorders in SARS-CoV-2 patients: a cross-sectional study. Clin Infect Dis.

841 Gilbert, M.A., Lin, B., Peterson, J., Jang, W., and Schwob, J.E. (2015). Neuregulin1 and ErbB
842 expression in the uninjured and regenerating olfactory mucosa. Gene Expression Patterns *19*,
843 108-119.

844 Gong, Q., Cheng, M., Chen, H., Liu, X., Si, Y., Yang, Y., Yuan, Y., Jin, C., Yang, W., He, F., *et*
845 *al.* (2011). Phospholipid scramblase 1 mediates hepatitis C virus entry into host cells. FEBS Lett
846 *585*, 2647-2652.

847 Harris, S.A., and Harris, E.A. (2018). Molecular Mechanisms for Herpes Simplex Virus Type 1
848 Pathogenesis in Alzheimer's Disease. Front Aging Neurosci *10*, 48.

849 Hegg, C.C., Jia, C., Chick, W.S., Restrepo, D., and Hansen, A. (2010). Microvillous cells
850 expressing IP3 receptor type 3 in the olfactory epithelium of mice. Eur J Neurosci *32*, 1632-
851 1645.

852 Hoffmann, M., Kleine-Weber, H., Schroeder, S., Kruger, N., Herrler, T., Erichsen, S.,
853 Schiergens, T.S., Herrler, G., Wu, N.H., Nitsche, A., *et al.* (2020). SARS-CoV-2 Cell Entry
854 Depends on ACE2 and TMPRSS2 and Is Blocked by a Clinically Proven Protease Inhibitor. Cell
855 *181*, 271-280 e278.

856 Hörl, D., Rojas Rusak, F., Preusser, F., Tillberg, P., Randel, N., Chhetri, R.K., Cardona, A.,
857 Keller, P.J., Harz, H., Leonhardt, H., *et al.* (2019). BigStitcher: reconstructing high-resolution
858 image datasets of cleared and expanded samples. Nature methods *16*, 870-874.

859 Juilfs, D.M., Fulle, H.J., Zhao, A.Z., Houslay, M.D., Garbers, D.L., and Beavo, J.A. (1997). A
860 subset of olfactory neurons that selectively express cGMP-stimulated phosphodiesterase (PDE2)
861 and guanylyl cyclase-D define a unique olfactory signal transduction pathway. Proc Natl Acad
862 Sci U S A *94*, 3388-3395.

863 Kim, B.E., Bin, L., Ye, Y.M., Ramamoorthy, P., and Leung, D.Y.M. (2013). IL-25 enhances
864 HSV-1 replication by inhibiting filaggrin expression, and acts synergistically with Th2 cytokines
865 to enhance HSV-1 replication. J Invest Dermatol *133*, 2678-2685.

866 Kolde, R. (2019). pheatmap: Pretty Heatmaps (cran.r-project.org).

867 Kopp, S.J., Banisadr, G., Glajch, K., Maurer, U.E., Grunewald, K., Miller, R.J., Osten, P., and
868 Spear, P.G. (2009). Infection of neurons and encephalitis after intracranial inoculation of herpes
869 simplex virus requires the entry receptor nectin-1. Proc Natl Acad Sci U S A *106*, 17916-17920.

870 Lee, W.J., Fu, R.M., Liang, C., and Sloan, R.D. (2018). IFITM proteins inhibit HIV-1 protein
871 synthesis. Sci Rep *8*, 14551.

872 Lemons, K., Fu, Z., Aoude, I., Ogura, T., Sun, J., Chang, J., Mbonu, K., Matsumoto, I.,
873 Arakawa, H., and Lin, W. (2017). Lack of TRPM5-Expressing Microvillous Cells in Mouse
874 Main Olfactory Epithelium Leads to Impaired Odor-Evoked Responses and Olfactory-Guided
875 Behavior in a Challenging Chemical Environment. eNeuro *4*.

876 Lemons, K., Fu, Z., Ogura, T., and Lin, W. (2020). TRPM5-expressing Microvillous Cells
877 Regulate Region-specific Cell Proliferation and Apoptosis During Chemical Exposure.
878 Neuroscience *434*, 171-190.

879 Li, H., Handsaker, B., Wysoker, A., Fennell, T., Ruan, J., Homer, N., Marth, G., Abecasis, G.,
880 Durbin, R., and Genome Project Data Processing, S. (2009). The Sequence Alignment/Map
881 format and SAMtools. Bioinformatics *25*, 2078-2079.

882 Li, M., Yang, J., Zhao, Y., Song, Y., Yin, S., Guo, J., Zhang, H., Wang, K., Wei, L., Li, S., *et al.*
883 (2020). MCPIP1 inhibits Hepatitis B virus replication by destabilizing viral RNA and negatively
884 regulates the virus-induced innate inflammatory responses. Antiviral Res *174*, 104705.

885 Liberles, S.D. (2015). Trace amine-associated receptors: ligands, neural circuits, and behaviors.
886 Current opinion in neurobiology *34*, 1-7.

887 Lin, R.J., Chu, J.S., Chien, H.L., Tseng, C.H., Ko, P.C., Mei, Y.Y., Tang, W.C., Kao, Y.T.,
888 Cheng, H.Y., Liang, Y.C., *et al.* (2014). MCPIP1 suppresses hepatitis C virus replication and
889 negatively regulates virus-induced proinflammatory cytokine responses. J Immunol *193*, 4159-
890 4168.

891 Lin, W., Ezekwe, E.A., Jr., Zhao, Z., Liman, E.R., and Restrepo, D. (2008). TRPM5-expressing
892 microvillous cells in the main olfactory epithelium. BMC Neurosci *9*, 114.

Lin, W., Margolskee, R., Donnert, G., Hell, S.W., and Restrepo, D. (2007). Olfactory neurons expressing transient receptor potential channel M5 (TRPM5) are involved in sensing semiochemicals. Proc Natl Acad Sci U S A *104*, 2471-2476.

Lopez, F., Delgado, R., Lopez, R., Bacigalupo, J., and Restrepo, D. (2014). Transduction for Pheromones in the Main Olfactory Epithelium Is Mediated by the Ca2+-Activated Channel TRPM5. J Neurosci *34*, 3268-3278.

Love, M.I., Huber, W., and Anders, S. (2014). Moderated estimation of fold change and dispersion for RNA-seq data with DESeq2. Genome Biol *15*, 550.

Luo, W., Zhang, J., Liang, L., Wang, G., Li, Q., Zhu, P., Zhou, Y., Li, J., Zhao, Y., Sun, N., *et al.* (2018). Phospholipid scramblase 1 interacts with influenza A virus NP, impairing its nuclear import and thereby suppressing virus replication. PLoS Pathog *14*, e1006851.

Luo, X.C., Chen, Z.H., Xue, J.B., Zhao, D.X., Lu, C., Li, Y.H., Li, S.M., Du, Y.W., Liu, Q., Wang, P., *et al.* (2019). Infection by the parasitic helminth Trichinella spiralis activates a Tas2r-mediated signaling pathway in intestinal tuft cells. Proc Natl Acad Sci U S A *116*, 5564-5569.

Maina, I.W., Workman, A.D., and Cohen, N.A. (2018). The role of bitter and sweet taste receptors in upper airway innate immunity: Recent advances and future directions. World J Otorhinolaryngol Head Neck Surg *4*, 200-208.

McGinty, J.W., Ting, H.-A., Billipp, T.E., Nadjsombati, M.S., Khan, D.M., Barrett, N.A., Liang, H.-E., Matsumoto, I., and von Moltke, J. (2020). Tuft-Cell-Derived Leukotrienes Drive Rapid Anti-helminth Immunity in the Small Intestine but Are Dispensable for Anti-protist Immunity. Immunity *52*, 528-541.e527.

McLaughlin, S.K., McKinnon, P.J., and Margolskee, R.F. (1992). Gustducin is a taste-cell-specific G protein closely related to the transducins. Nature *357*, 563-569.

Meyerson, N.R., Zhou, L., Guo, Y.R., Zhao, C., Tao, Y.J., Krug, R.M., and Sawyer, S.L. (2017). Nuclear TRIM25 Specifically Targets Influenza Virus Ribonucleoproteins to Block the Onset of RNA Chain Elongation. Cell Host Microbe *22*, 627-638 e627.

Mogha, A., Harty, B.L., Carlin, D., Joseph, J., Sanchez, N.E., Suter, U., Piao, X., Cavalli, V., and Monk, K.R. (2016). Gpr126/Adgrg6 Has Schwann Cell Autonomous and Nonautonomous Functions in Peripheral Nerve Injury and Repair. The Journal of Neuroscience *36*, 12351.

Mombaerts, P., Wang, F., Dulac, C., Chao, S.K., Nemes, A., Mendelsohn, M., Edmondson, J., and Axel, R. (1996). Visualizing an olfactory sensory map. Cell *87*, 675-686.

Narayana, S.K., Helbig, K.J., McCartney, E.M., Eyre, N.S., Bull, R.A., Eltahla, A., Lloyd, A.R., and Beard, M.R. (2015). The Interferon-induced Transmembrane Proteins, IFITM1, IFITM2, and IFITM3 Inhibit Hepatitis C Virus Entry. J Biol Chem *290*, 25946-25959.

927 Noyce, R.S., and Richardson, C.D. (2012). Nectin 4 is the epithelial cell receptor for measles
928 virus. Trends Microbiol *20*, 429-439.

929 O'Leary, C.E., Schneider, C., and Locksley, R.M. (2019). Tuft Cells-Systemically Dispersed
930 Sensory Epithelia Integrating Immune and Neural Circuitry. Annu Rev Immunol *37*, 47-72.

931 Ogura, T., Szebenyi, S.A., Krosnowski, K., Sathyanesan, A., Jackson, J., and Lin, W. (2011).
932 Cholinergic microvillous cells in the mouse main olfactory epithelium and effect of acetylcholine
933 on olfactory sensory neurons and supporting cells. J Neurophysiol *106*, 1274-1287.

934 Omura, M., and Mombaerts, P. (2014). Trpc2-Expressing Sensory Neurons in the Main
935 Olfactory Epithelium of the Mouse. Cell Reports *8*, 583-595.

936 Oshimoto, A., Wakabayashi, Y., Garske, A., Lopez, R., Rolen, S., Flowers, M., Arevalo, N., and
937 Restrepo, D. (2013). Potential role of transient receptor potential channel M5 in sensing putative
938 pheromones in mouse olfactory sensory neurons. PLoS One *8*, e61990.

939 Parma, V., Ohla, K., Veldhuizen, M.G., Niv, M.Y., Kelly, C.E., Bakke, A.J., Cooper, K.W.,
940 Bouysset, C., Pirastu, N., Dibattista, M., *et al.* (2020). More than smell – COVID-19 is
941 associated with severe impairment of smell, taste, and chemesthesis. Chemical Senses *45*, 609-
942 622.

943 Patro, R., Duggal, G., Love, M.I., Irizarry, R.A., and Kingsford, C. (2017). Salmon provides fast
944 and bias-aware quantification of transcript expression. Nature methods *14*, 417-419.

945 Perniss, A., Liu, S., Boonen, B., Keshavarz, M., Ruppert, A.L., Timm, T., Pfeil, U., Soultanova,
946 A., Kusumakshi, S., Delventhal, L., *et al.* (2020). Chemosensory Cell-Derived Acetylcholine
947 Drives Tracheal Mucociliary Clearance in Response to Virulence-Associated Formyl Peptides.
948 Immunity *52*, 683-699 e611.

949 Petermann, P., Rahn, E., Thier, K., Hsu, M.J., Rixon, F.J., Kopp, S.J., and Knebel-Morsdorf, D.
950 (2015). Role of Nectin-1 and Herpesvirus Entry Mediator as Cellular Receptors for Herpes
951 Simplex Virus 1 on Primary Murine Dermal Fibroblasts. J Virol *89*, 9407-9416.

952 Pomaznoy, M., Ha, B., and Peters, B. (2018). GOnet: a tool for interactive Gene Ontology
953 analysis. BMC Bioinformatics *19*, 470.

954 Pyrski, M., Eckstein, E., Schmid, A., Bufe, B., Weiss, J., Chubanov, V., Boehm, U., and Zufall,
955 F. (2017). Trpm5 expression in the olfactory epithelium. Mol Cell Neurosci *80*, 75-88.

956 Pyrski, M., Tusty, M., Eckstein, E., Oboti, L., Rodriguez-Gil, D.J., Greer, C.A., and Zufall, F.
957 (2018). P/Q Type Calcium Channel Cav2.1 Defines a Unique Subset of Glomeruli in the Mouse
958 Olfactory Bulb. Frontiers in Cellular Neuroscience *12*, 295.

959 Rane, C.K., Jackson, S.R., Pastore, C.F., Zhao, G., Weiner, A.I., Patel, N.N., Herbert, D.R.,
960 Cohen, N.A., and Vaughan, A.E. (2019). Development of solitary chemosensory cells in the
961 distal lung after severe influenza injury. Am J Physiol Lung Cell Mol Physiol *316*, L1141-
962 L1149.

963 Sapoznik, E., Chang, B.-J., Huh, J., Ju, R.J., Azarova, E.V., Pohlkamp, T., Welf, E.S.,
964 Broadbent, D., Carisey, A.F., Stehbens, S.J., *et al.* (2020). A Versatile Oblique Plane Microscope
965 for Large-Scale and High-Resolution Imaging of Subcellular Dynamics. eLife *9*, e57681.

966 Saunders, C.J., Christensen, M., Finger, T.E., and Tizzano, M. (2014). Cholinergic
967 neurotransmission links solitary chemosensory cells to nasal inflammation. Proc Natl Acad Sci U
968 S A *111*, 6075-6080.

969 Sayers, C.L., and Elliott, G. (2016). Herpes Simplex Virus 1 Enters Human Keratinocytes by a
970 Nectin-1-Dependent, Rapid Plasma Membrane Fusion Pathway That Functions at Low
971 Temperature. J Virol *90*, 10379-10389.

972 Sepahi, A., Kraus, A., Casadei, E., Johnston, C.A., Galindo-Villegas, J., Kelly, C., García-
973 Moreno, D., Muñoz, P., Mulero, V., Huertas, M., *et al.* (2019). Olfactory sensory neurons
974 mediate ultrarapid antiviral immune responses in a TrkA-dependent manner. Proceedings of the
975 National Academy of Sciences *116*, 12428.

976 Shestakov, A., Jenssen, H., Nordstrom, I., and Eriksson, K. (2012). Lactoferricin but not
977 lactoferrin inhibit herpes simplex virus type 2 infection in mice. Antiviral Res *93*, 340-345.

978 Shukla, N.D., Tiwari, V., and Valyi-Nagy, T. (2012). Nectin-1-specific entry of herpes simplex
979 virus 1 is sufficient for infection of the cornea and viral spread to the trigeminal ganglia. Mol Vis
980 *18*, 2711-2716.

981 Singh, B.K., Hornick, A.L., Krishnamurthy, S., Locke, A.C., Mendoza, C.A., Mateo, M., Miller-
982 Hunt, C.L., Cattaneo, R., and Sinn, P.L. (2015). The Nectin-4/Afadin Protein Complex and
983 Intercellular Membrane Pores Contribute to Rapid Spread of Measles Virus in Primary Human
984 Airway Epithelia. J Virol *89*, 7089-7096.

985 Singh, B.K., Li, N., Mark, A.C., Mateo, M., Cattaneo, R., and Sinn, P.L. (2016). Cell-to-Cell
986 Contact and Nectin-4 Govern Spread of Measles Virus from Primary Human Myeloid Cells to
987 Primary Human Airway Epithelial Cells. J Virol *90*, 6808-6817.

988 Soneson, C., Love, M.I., and Robinson, M.D. (2015). Differential analyses for RNA-seq:
989 transcript-level estimates improve gene-level inferences. F1000Res *4*, 1521.

990 Thompson, J.A., Salcedo, E., Restrepo, D., and Finger, T.E. (2012). Second-order input to the
991 medial amygdala from olfactory sensory neurons expressing the transduction channel TRPM5. J
992 Comp Neurol *520*, 1819-1830.

993 Ting, H.-A., and von Moltke, J. (2019). The Immune Function of Tuft Cells at Gut Mucosal
994 Surfaces and Beyond. The Journal of Immunology *202*, 1321.

995 Tizzano, M., Gulbransen, B.D., Vandenbeuch, A., Clapp, T.R., Herman, J.P., Sibhatu, H.M.,
996 Churchill, M.E., Silver, W.L., Kinnamon, S.C., and Finger, T.E. (2010). Nasal chemosensory
997 cells use bitter taste signaling to detect irritants and bacterial signals. Proc Natl Acad Sci U S A
998 *107*, 3210-3215.

Ualiyeva, S., Hallen, N., Kanaoka, Y., Ledderose, C., Matsumoto, I., Junger, W., Barrett, N.A., and Bankova, L.G. (2020). Airway brush cells generate cysteinyl leukotrienes through the ATP sensor P2Y2. Science immunology *5*.

Valimaa, H., Tenovuo, J., Waris, M., and Hukkanen, V. (2009). Human lactoferrin but not lysozyme neutralizes HSV-1 and inhibits HSV-1 replication and cell-to-cell spread. Virol J *6*, 53.

van der Linden, C., Jakob, S., Gupta, P., Dulac, C., and Santoro, S.W. (2018). Sex separation induces differences in the olfactory sensory receptor repertoires of male and female mice. Nat Commun *9*, 5081.

Villar, P.S., Delgado, R., Vergara, C., Reyes, J.G., and Bacigalupo, J. (2017). Energy Requirements of Odor Transduction in the Chemosensory Cilia of Olfactory Sensory Neurons Rely on Oxidative Phosphorylation and Glycolytic Processing of Extracellular Glucose. J Neurosci *37*, 5736-5743.

von Moltke, J., Ji, M., Liang, H.E., and Locksley, R.M. (2016). Tuft-cell-derived IL-25 regulates an intestinal ILC2-epithelial response circuit. Nature *529*, 221-225.

Wilen, C.B., Lee, S., Hsieh, L.L., Orchard, R.C., Desai, C., Hykes, B.L., McAllaster, M.R., Balce, D.R., Feehley, T., Brestoff, J.R., *et al.* (2018). Tropism for tuft cells determines immune promotion of norovirus pathogenesis. Science *360*, 204.

1016 Yamaguchi, T., Yamashita, J., Ohmoto, M., Aoude, I., Ogura, T., Luo, W., Bachmanov, A.A.,
1017 Lin, W., Matsumoto, I., and Hirota, J. (2014). Skn-1a/Pou2f3 is required for the generation of
1018 Trpm5-expressing microvillous cells in the mouse main olfactory epithelium. BMC Neurosci *15*,
1019 13.

1020 Yamashita, J., Ohmoto, M., Yamaguchi, T., Matsumoto, I., and Hirota, J. (2017). Skn-1a/Pou2f3
1021 functions as a master regulator to generate Trpm5-expressing chemosensory cells in mice. PLoS
1022 One *12*, e0189340.

1023 Yan, C.H., Faraji, F., Prajapati, D.P., Boone, C.E., and DeConde, A.S. (2020a). Association of
1024 chemosensory dysfunction and Covid-19 in patients presenting with influenza-like symptoms.
1025 Int Forum Allergy Rhinol.

1026 Yan, C.H., Faraji, F., Prajapati, D.P., Ostrander, B.T., and DeConde, A.S. (2020b). Self-reported
1027 olfactory loss associates with outpatient clinical course in Covid-19. Int Forum Allergy Rhinol.

1028 Yang, J., Zhu, X., Liu, J., Ding, X., Han, M., Hu, W., Wang, X., Zhou, Z., and Wang, S. (2012).
1029 Inhibition of Hepatitis B virus replication by phospholipid scramblase 1 in vitro and in vivo.
1030 Antiviral Res *94*, 9-17.

1031 Yu, J., Li, M., Wilkins, J., Ding, S., Swartz, T.H., Esposito, A.M., Zheng, Y.M., Freed, E.O.,
1032 Liang, C., Chen, B.K., *et al.* (2015). IFITM Proteins Restrict HIV-1 Infection by Antagonizing
1033 the Envelope Glycoprotein. Cell Rep *13*, 145-156.

1034 Zerbino, D.R., Achuthan, P., Akanni, W., Amode, M.R., Barrell, D., Bhai, J., Billis, K.,
1035 Cummins, C., Gall, A., Giron, C.G., *et al.* (2018). Ensembl 2018. Nucleic Acids Res *46*, D754-
1036 D761.

1037 Zhang, Y., Hoon, M.A., Chandrashekar, J., Mueller, K.L., Cook, B., Wu, D., Zuker, C.S., and
1038 Ryba, N.J. (2003). Coding of sweet, bitter, and umami tastes: different receptor cells sharing
1039 similar signaling pathways. Cell *112*, 293-301.

1040 Zheng, Y., Qin, Z., Ye, Q., Chen, P., Wang, Z., Yan, Q., Luo, Z., Liu, X., Zhou, Y., Xiong, W.,
1041 *et al.* (2014). Lactoferrin suppresses the Epstein-Barr virus-induced inflammatory response by
1042 interfering with pattern recognition of TLR2 and TLR9. Lab Invest *94*, 1188-1199.

1043 Zheng, Y., Zhang, W., Ye, Q., Zhou, Y., Xiong, W., He, W., Deng, M., Zhou, M., Guo, X.,
1044 Chen, P., *et al.* (2012). Inhibition of Epstein-Barr virus infection by lactoferrin. J Innate Immun
1045 *4*, 387-398.

1046 Ziegler, C.G.K., Allon, S.J., Nyquist, S.K., Mbano, I.M., Miao, V.N., Tzouanas, C.N., Cao, Y.,
1047 Yousif, A.S., Bals, J., Hauser, B.M., *et al.* (2020). SARS-CoV-2 receptor ACE2 is an interferon-
1048 stimulated gene in human airway epithelial cells and is detected in specific cell subsets across
1049 tissues. Cell *181*, 1016-1035.

1050
1051

Figure 1. Fluorescence activated sorting (FACS) of cells isolated from the olfactory epithelium.

a. TRPM5 promoter driven expression of eGFP and OMP promoter driven expression of mCherry in the olfactory epithelium. Expression of eGFP is found both in MVCs that do not express mCherry (asterisk) and in OSNs double labeled with eGFP and mCherry (arrow). **i.** Composite, **ii.** eGFP, **iii.** mCherry, **iv**. Composite magnification. Magenta: mCherry, green: eGFP. Scale bar: i-iii, 50 μm, iv, 10 μm.

b. Schematic of RNA-seq process from tissue to RNA extraction. Mouse OE was dissociated into single cells and sorted via FACS. RNA was extracted from each of the resulting cell populations.

c. Two isolated OSNs differing in eGFP expression. Magenta: mCherry, green: eGFP. Scale bar: 10 μm.

d. Distribution of mCherry and eGFP fluorescence intensity for FACS-sorted cells. Three cell populations were isolated for RNAseq: Cells with low OMP promoter-driven mCherry expression and high TRPM5 promoter-driven eGFP expression (MVC_eGFP cells), cells with high OMP promoter-driven mCherry and low eGFP expression (OSN_eGFP- cells) and cells with eGFP expression of the same magnitude as MVC_eGFP cells and high OMP promoter-driven mCherry expression (OSN_eGFP+ cells). The number of cells collected for this FACS run were: OSN_eGFP-s 1,500,000, OSN_eGFP+s 5336 and MVC_eGFP cells 37,178.

e. qPCR levels (normalized to levels 18s RNA) for expression of transcripts encoding for OMP (**i**), TRPM5 (**ii**), eGFP (**iii**) and ChAT (**iv**). The asterisks denote significant differences tested with either t-test or ranksum with p-values below the significance p-value corrected for multiple comparisons using the false discovery rate (pFDR)(Curran-Everett, 2000). pFDR is 0.033 for

OMP, 0.05 for TRPM5, 0.05 for eGFP and 0.03 for ChAT, n=8 for OMP OSN_eGFP-s, 4 for OMP OSN_eGFP+s and 4 for MVC_eGFP cells.

Figure 2. RNAseq comparison of MVC_eGFP vs. OSN_eGFP- cells.

a. Heatmaps showing hierarchical clustering of the top 10 upregulated and top 10 downregulated genes identified by DESeq2.

b. Heatmaps showing hierarchical clustering of the 550 olfactory receptor genes identified by DESeq2 as expressed in OSN_eGFP- cells. For both a and b, row and column order were determined automatically by the *pHeatmap* package in R. Row values were centered and scaled using 'scale = "row"' within *pHeatmap*.

c. Volcano plot of all olfactory receptors, demonstrating the large number of enriched olfactory receptors in the OSN_eGFP- population.

d. Hierarchical clustering of transcripts for taste transduction and transcripts expressed in canonical and non-canonical OSNs identified by RNAseq as significantly different in expression between MVC_eGFP and OSN_eGFP- cells. The non-canonical OSNs considered here included guanilyl-cyclase D (GC-D) OSNs (Juilfs et al., 1997), Trpc2 OSNs (Omura and Mombaerts, 2014), Cav2.1 OSNs (Pyrski et al., 2018), and OSNs expressing trace amine-associated receptors (Taars) (Liberles, 2015). Transcripts identified by DESeq2.

e. Gene ontology (GO) term enrichment for synaptic vesicle or chemosensory-related GOs was calculated from differentially expressed genes using *TopGO* in R. An enrichment value for genes with Fischer p value <0.05 was calculated by dividing the number of expressed genes within the GO term by the number expected genes (by random sampling, determined by *TopGO*).

Figure 3. Significant differences in virally-related, immune and inflammation gene ontology lists between MVC_eGFP and OSN_eGFP-. a. Gene ontology (GO) term enrichment was calculated from differentially expressed genes using *TopGO* in R for OSN_eGFP- vs. MVC_eGFP cells. An enrichment value for genes with Fischer p value <0.05 was calculated by dividing the number of expressed genes within the GO term by the number expected genes (by random sampling, determined by *TopGO*). Heatmap show hierarchical clustering of significantly differentially expressed genes identified by DESeq2. **b.** Significantly differences in virally-related genes within the MVC_eGFP cells compared to OSN_eGFP-.

Figure 4. RNAseq comparison of OSN_eGFP+ to both MVC_eGFP and OSN_eGFP- cells. **a.** Heatmap showing the top upregulated genes (excluding Olfrs) that are expressed in OSN_eGFP+ cells 4 fold higher than OSN_eGFP- AND MVC_eGFP cells. Additional criteria for inclusion was mean of expression > standard deviation of expression and mean of expression greater than 100.

b. Heatmap showing all *Olfr* genes differentially expressed between OSN_eGFP+ and OSN_eGFP- cells identified by DESeq2. MVC_eGFP cells did not express Olfrs.

For both a and b, row and column order were determined automatically by the *pHeatmap* package in R. For each data point relative expression was calculated by subtracting the average row value from each individual value.

c. Volcano plot of all Olfactory receptors, demonstrating the small number of enriched olfactory receptors in the OSN_eGFP+ population.

d. Hierarchical clustering of transcripts for taste transduction and transcripts expressed in canonical and non-canonical OSNs identified by RNAseq as significantly different in expression

between the cell groups. We compared expression of transcripts involved in taste transduction, canonical olfactory transduction, and non-canonical OSNs. The non-canonical OSNs considered here included guanilyl-cyclase D (GC-D) OSNs (Juilfs et al., 1997), Trpc2 OSNs (Omura and Mombaerts, 2014), Cav2.1 OSNs (Pyrski et al., 2018), and OSNs expressing trace amine-associated receptors (Taars) (Liberles, 2015). Transcripts identified by DESeq2.

Figure 5. *In situ* hybridization chain reaction finds strong TRPM5 mRNA expression in MVC_eGFP cells, but not in the nuclear OSN layer.

a. In situ for TRPM5 (yellow) and OMP (magenta) transcripts in the olfactory epithelium of TRPM5-GFP mice (GFP is green) shows strong label for TRPM5 in MVCs (asterisks) and sparse labeling in the OSN nuclear layer (arrows). The scale bar is 20 μm.

b. In situ for TRPM5 (yellow) and OMP (magenta) transcripts in the olfactory epithelium of TRPM5-GFP x TRPM5-knockout mice (GFP is green) shows no label for TRPM5 in GFP-positive MVCs (asterisks) and does show sparse labeling in the OSN nuclear layer (arrows). The scale bar is 20 μm.

Figure 6. Model depicting the role for microvillous cells involvement in the olfactory epithelium innate immune response to viral infection. 1) Secreted or cell surface glycoproteins constitute a first barrier preventing virus entry. 2) When reaching MVC_eGFP, viruses can encounter three types of membrane proteins: adhesion molecules that trigger intracellular signaling upon viral recognition (black rectangle), transmembrane proteins that block virus entry (black circle), viral receptors allowing virus entry (grey circle). 3) MVC_eGFP express numerous transcriptional factors involved in the inhibition of viral replication. 4)

Cytosolic viral RNA sensing induces the production of type I interferons. 5) A possible signaling pathway leading to intracellular calcium increase, TRPM5 activation and Na^+-mediated vesicle release. Acetylcholine can activate neighboring sustentacular cells and underlying trigeminal fibers. 6) Eicosanoids synthesis, along with IL-25 production, can recruit and activate group 2 innate lymphoid cells, which are key controllers of type 2 inflammation. 7) GPR126 activation results in NFkB activation and TNFα production. TNFα can directly activate macrophages. TNFα also induces a change in the function of horizontal basal cells, switching their phenotype from neuroregeneration to immune defense. 8) Interferons and cytokines can in turn activate antiviral immune response in neighboring MVC_eGFP.

Name	OSN_eGFP-	OSN_eGFP+	MVC_eGFP	p-value adjusted
Olfr292	3.61	959	4.29	6.35E-09
Olfr282	2.05	486	0	8.01E-05
Olfr1434	53.3	7730	0	9.71E-16
Olfr390	101	10800	43.1	1.56E-16
Olfr305	6.14	612	0	6.3E-12
Olfr293	6.96	664	16.9	1.42E-07
Olfr378	3.41	322	0	1.1E-06
Olfr128	39.6	3660	12.7	7.33E-14
Olfr344	16.2	1050	0	1.4E-11
Olfr307	7.59	393	0	3.76E-06
Olfr391	156	8000	9.79	1.01E-15
Olfr299	13.1	651	0	4.58E-09
Olfr142	36.4	1720	3.77	1.62E-08
Olfr1	147	5720	52.7	3.08E-10
Olfr1279	16.4	552	10.9	3.52E-07
Olfr39	13.8	388	21	2.81E-06
Olfr1447	64.1	1610	0	1.23E-07
Olfr728	2150	45700	320	6.13E-22
Olfr727	560	11000	179	1.64E-07
Olfr1555-ps1	10.1	175	0	0.0397
Olfr346	27.6	465	0	3.85E-05
Olfr1228	533	5320	35.4	3.09E-08
Olfr1181	87.4	766	4.61	0.000766
Olfr943	97.1	844	2.89	0.000886
Olfr298	60.1	509	0	0.00132

Table 1. Levels of expression and adjusted p-value for the olfactory receptor genes whose levels are significantly higher in OSN_eGFP+ compared to OSN_eGFP-. These olfactory receptors had an adjusted p-value for expression level difference between OSN_eGFP+ compared to OSN_eGFP- and had a fold change > 4 and average expression > 100 counts.

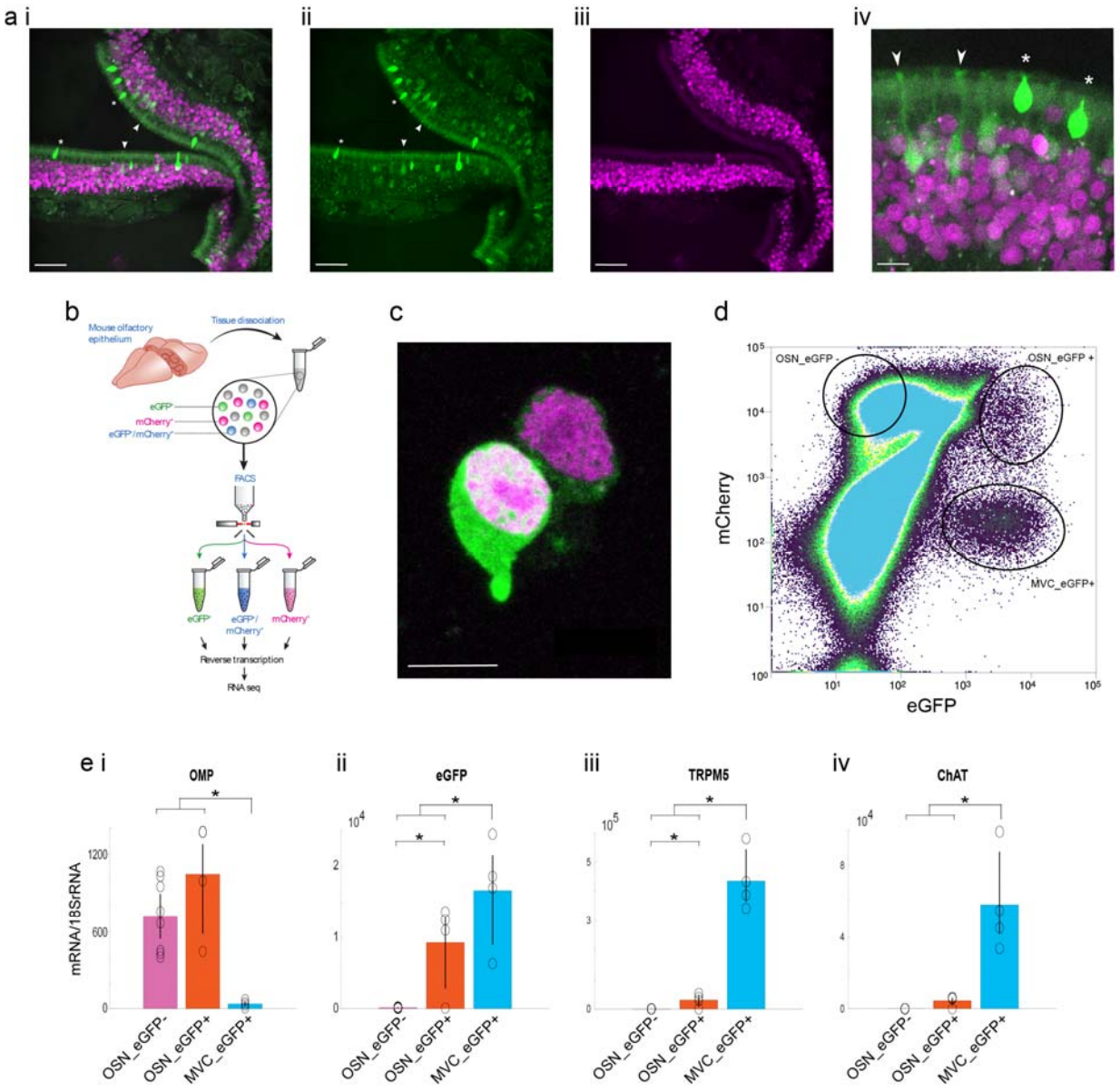

Figure 1. Fluorescence activated sorting (FACS) of cells isolated from the olfactory epithelium.

a. TRPM5 promoter driven expression of eGFP and OMP promoter driven expression of mCherry in the olfactory epithelium. Expression of eGFP is found both in MVCs that do not express mCherry (asterisk) and in OSNs double labeled with eGFP and mCherry (arrow). **i.** Composite, **ii.** eGFP, **iii.** mCherry, **iv**. Composite magnification. Magenta: mCherry, green: eGFP. Scale bar: i-iii, 50 μm, iv, 10 μm.

b. Schematic of RNA-seq process from tissue to RNA extraction. Mouse OE was dissociated into single cells and sorted via FACS. RNA was extracted from each of the resulting cell populations.

c. Two isolated OSNs differing in eGFP expression. Magenta: mCherry, green: eGFP. Scale bar: 10 μm.

d. Distribution of mCherry and eGFP fluorescence intensity for FACS-sorted cells. Three cell populations were isolated for RNAseq: Cells with low OMP promoter-driven mCherry expression and high TRPM5 promoter-driven eGFP expression (MVC_eGFP cells), cells with high OMP promoter-driven mCherry and low eGFP expression (OSN_eGFP- cells) and cells with eGFP expression of the same magnitude as MVC_eGFP cells and high OMP promoter-driven mCherry expression (OSN_eGFP+ cells). The number of cells collected for this FACS run were: OSN_eGFP-s 1,500,000, OSN_eGFP+s 5336 and MVC_eGFP cells 37,178.

e. qPCR levels (normalized to levels 18s RNA) for expression of transcripts encoding for OMP (**i**), TRPM5 (**ii**), eGFP (**iii**) and ChAT (**iv**). The asterisks denote significant differences tested with either t-test or ranksum with p-values below the significance p-value corrected for multiple comparisons using the false discovery rate (pFDR)(Curran-Everett, 2000). pFDR is 0.033 for OMP, 0.05 for TRPM5, 0.05 for eGFP and 0.03 for ChAT, n=8 for OMP OSN_eGFP-s, 4 for OMP OSN_eGFP+s and 4 for MVC_eGFP cells.

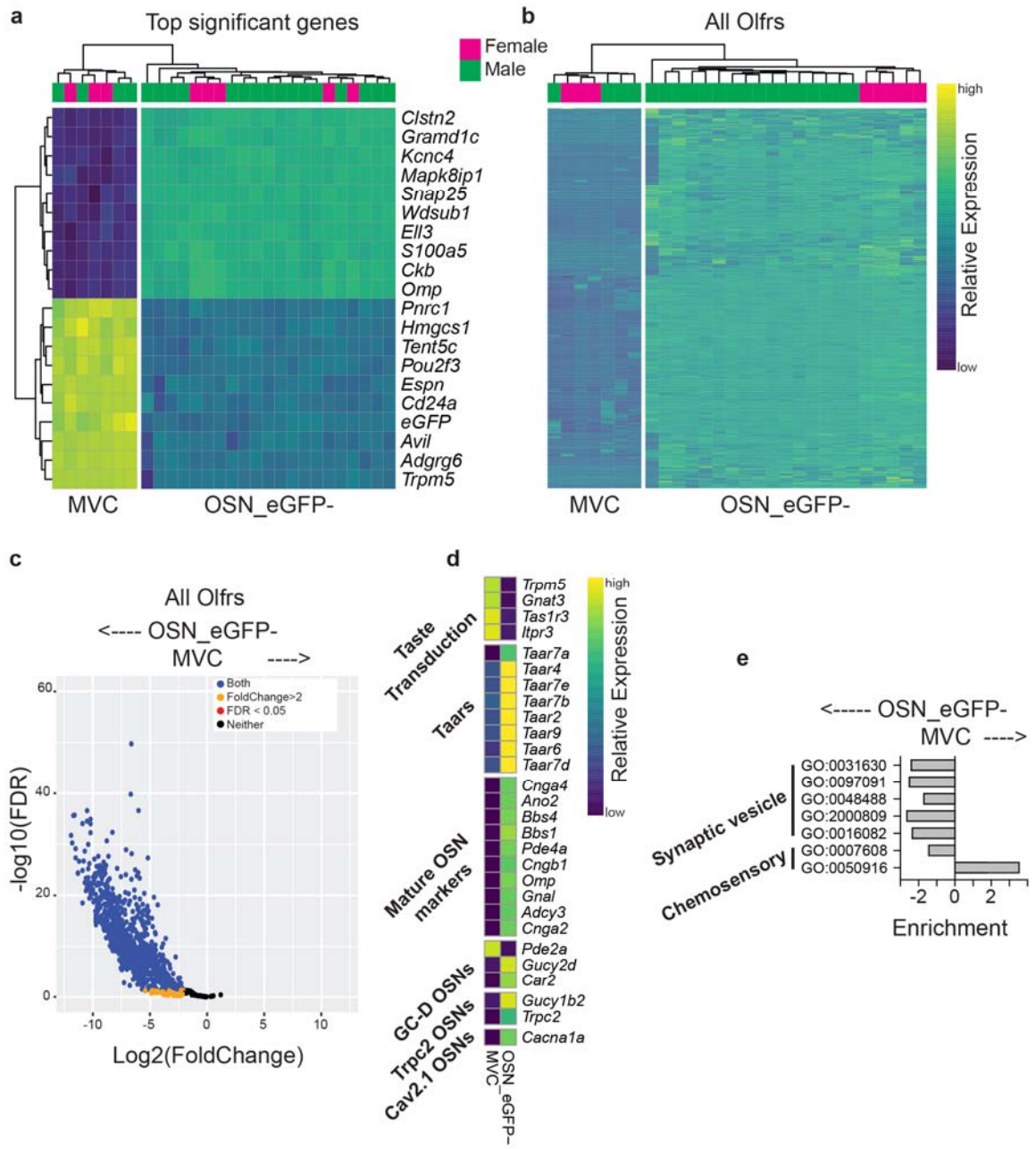

Figure 2. RNAseq comparison of MVC_eGFP vs. OSN_eGFP- cells.

a. Heatmaps showing hierarchical clustering of the top 10 upregulated and top 10 downregulated genes identified by DESeq2.

b. Heatmaps showing hierarchical clustering of the 550 olfactory receptor genes identified by DESeq2 as expressed in OSN_eGFP- cells. For both a and b, row and column order were

1196 determined automatically by the *pHeatmap* package in R. Row values were centered and scaled
1197 using 'scale = "row"' within *pHeatmap*.
1198 **c.** Volcano plot of all olfactory receptors, demonstrating the large number of enriched olfactory
1199 receptors in the OSN_eGFP- population.
1200 **d.** Hierarchical clustering of transcripts for taste transduction and transcripts expressed in
1201 canonical and non-canonical OSNs identified by RNAseq as significantly different in expression
1202 between MVC_eGFP and OSN_eGFP- cells. The non-canonical OSNs considered here included
1203 guanilyl-cyclase D (GC-D) OSNs (Juilfs et al., 1997), Trpc2 OSNs (Omura and Mombaerts,
1204 2014), Cav2.1 OSNs (Pyrski et al., 2018), and OSNs expressing trace amine-associated receptors
1205 (Taars) (Liberles, 2015). Transcripts identified by DESeq2.
1206 **e.** Gene ontology (GO) term enrichment for synaptic vesicle or chemosensory-related GOs was
1207 calculated from differentially expressed genes using *TopGO* in R. An enrichment value for genes
1208 with Fischer p value <0.05 was calculated by dividing the number of expressed genes within the
1209 GO term by the number expected genes (by random sampling, determined by *TopGO*).
1210

1211

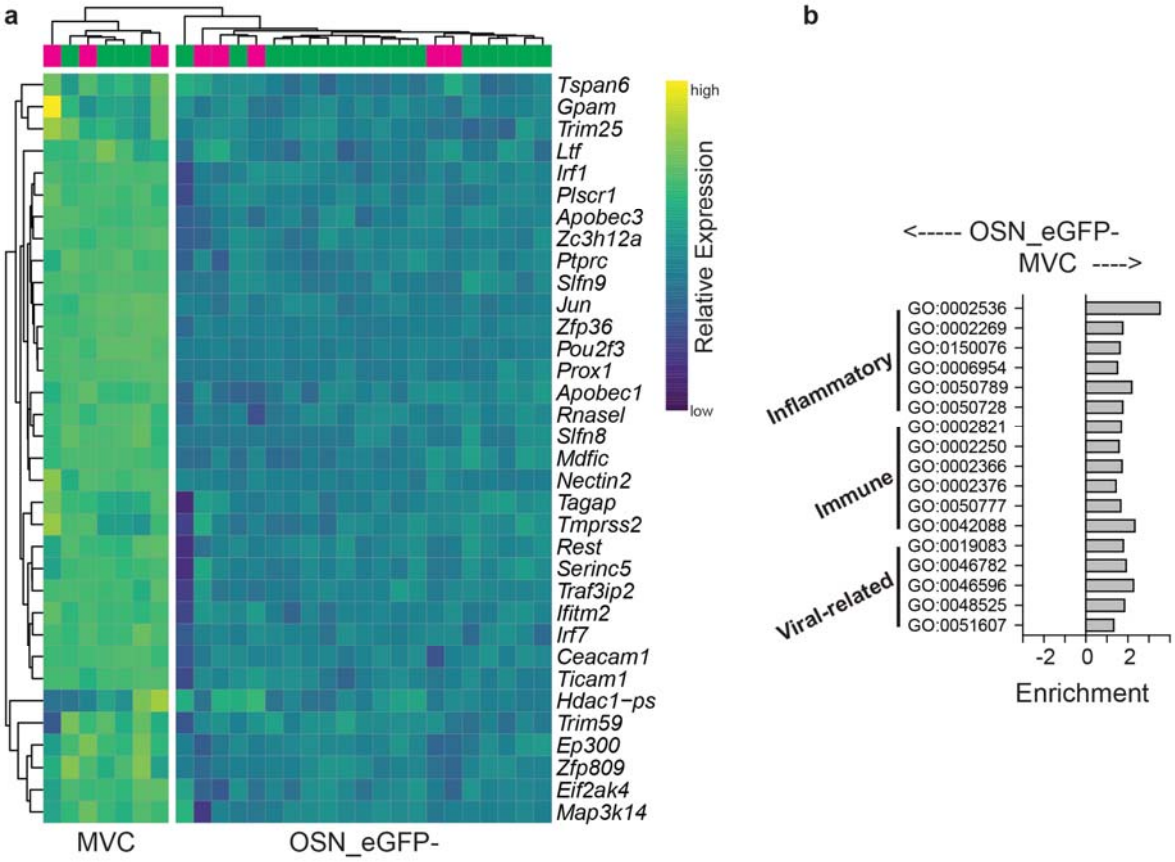

1212

1213 **Figure 3. Significant differences in virally-related, immune and inflammation gene**

1214 **ontology lists between MVC_eGFP and OSN_eGFP-. a.** Gene ontology (GO) term enrichment

1215 was calculated from differentially expressed genes using *TopGO* in R for OSN_eGFP- vs.

1216 MVC_eGFP cells. An enrichment value for genes with Fischer p value <0.05 was calculated by

1217 dividing the number of expressed genes within the GO term by the number expected genes (by

1218 random sampling, determined by *TopGO*). Heatmap show hierarchical clustering of significantly

1219 differentially expressed genes identified by DESeq2. **b.** Significantly differences in virally-

1220 related genes within the MVC_eGFP cells compared to OSN_eGFP-.

1221

1222

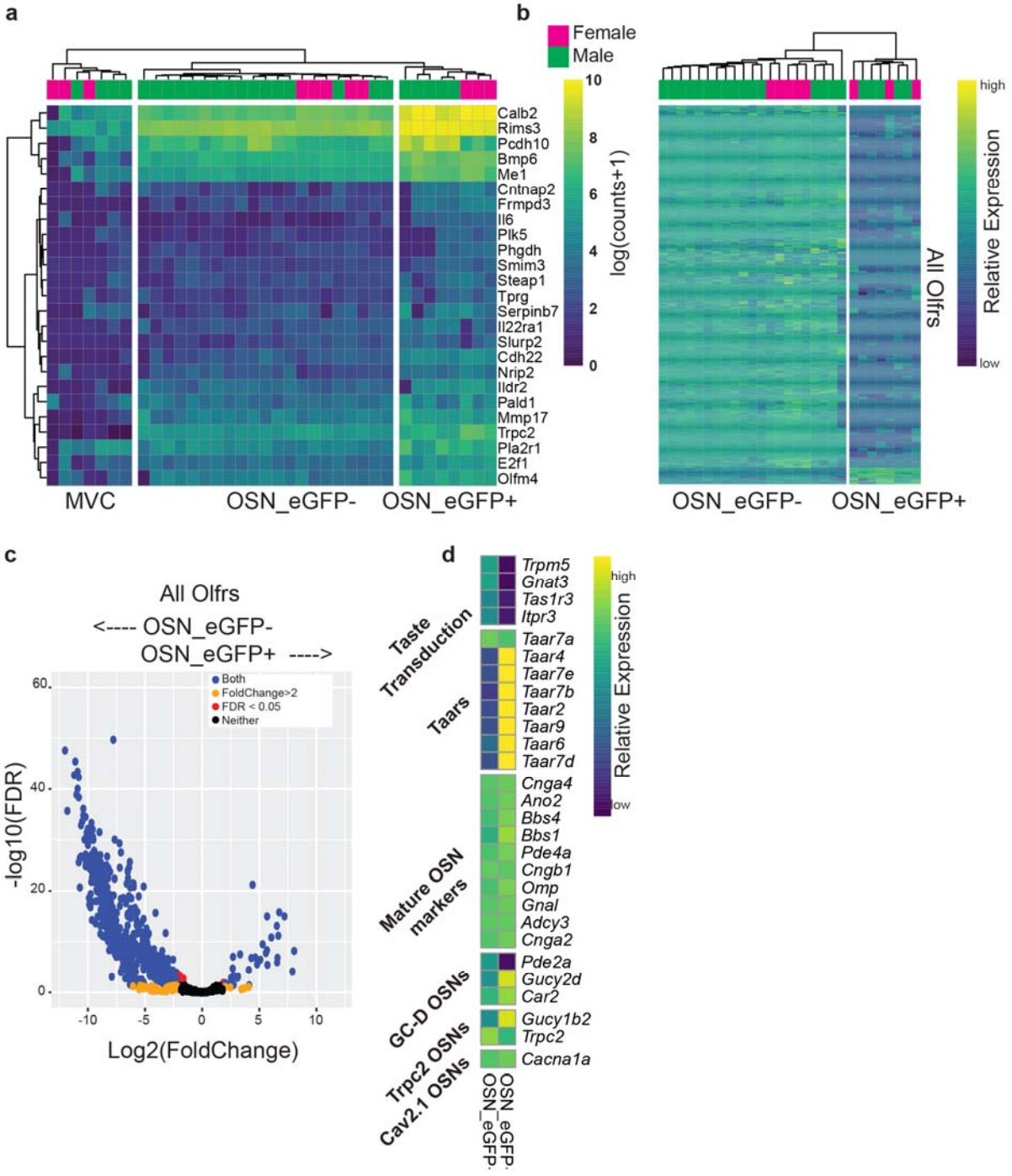

1223

1224 **Figure 4. RNAseq comparison of OSN_eGFP+ to both MVC_eGFP and OSN_eGFP- cells.**

1225 **a.** Heatmap showing the top upregulated genes (excluding Olfrs) that are expressed in

1226 OSN_eGFP+ cells 4 fold higher than OSN_eGFP- AND MVC_eGFP cells. Additional criteria

for inclusion was mean of expression > standard deviation of expression and mean of expression greater than 100.

b. Heatmap showing all *Olfr* genes differentially expressed between OSN_eGFP+ and OSN_eGFP- cells identified by DESeq2. MVC_eGFP cells did not express Olfrs. For both a and b, row and column order were determined automatically by the *pHeatmap* package in R. For each data point relative expression was calculated by subtracting the average row value from each individual value.

c. Volcano plot of all Olfactory receptors, demonstrating the small number of enriched olfactory receptors in the OSN_eGFP+ population.

d. Hierarchical clustering of transcripts for taste transduction and transcripts expressed in canonical and non-canonical OSNs identified by RNAseq as significantly different in expression between the cell groups. We compared expression of transcripts involved in taste transduction, canonical olfactory transduction, and non-canonical OSNs. The non-canonical OSNs considered here included guanilyl-cyclase D (GC-D) OSNs (Juilfs et al., 1997), Trpc2 OSNs (Omura and Mombaerts, 2014), Cav2.1 OSNs (Pyrski et al., 2018), and OSNs expressing trace amine-associated receptors (Taars) (Liberles, 2015). Transcripts identified by DESeq2.

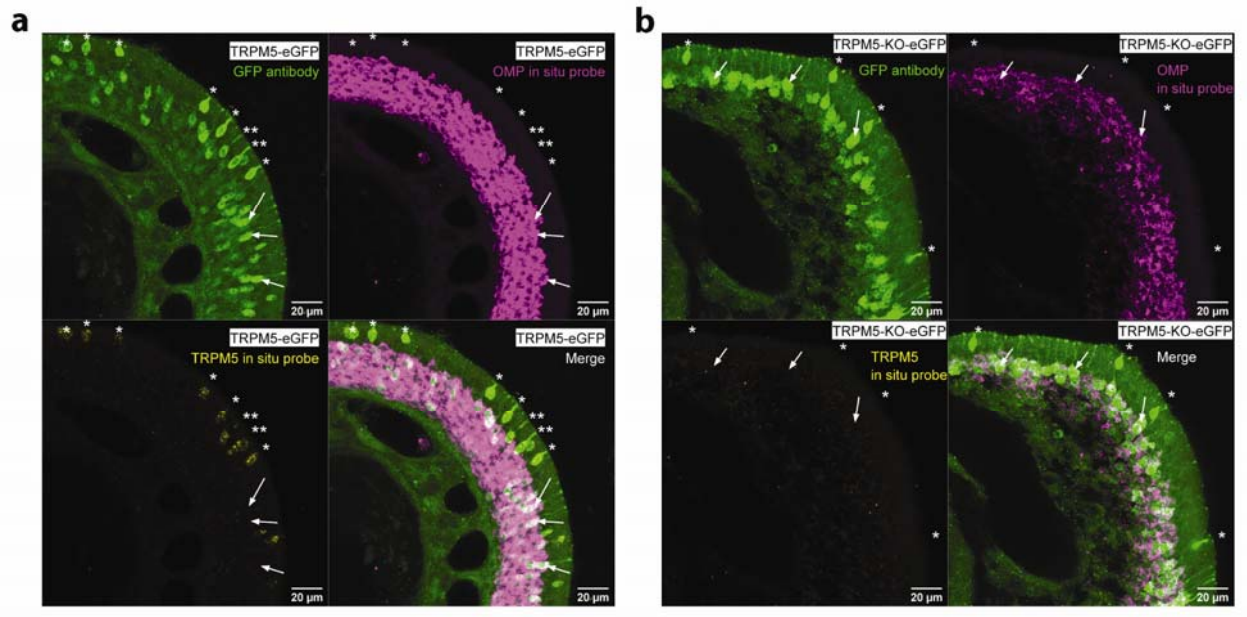

1244

1245

1246 **Figure 5. *In situ* hybridization chain reaction finds strong TRPM5 mRNA expression in**

1247 **MVC_eGFP cells, but not in the nuclear OSN layer.**

1248 **a.** In situ for TRPM5 (yellow) and OMP (magenta) transcripts in the olfactory epithelium of

1249 TRPM5-GFP mice (GFP is green) shows strong label for TRPM5 in MVCs (asterisks) and

1250 sparse labeling in the OSN nuclear layer (arrows). The scale bar is 20 µm.

1251 **b.** In situ for TRPM5 (yellow) and OMP (magenta) transcripts in the olfactory epithelium of

1252 TRPM5-GFP x TRPM5-knockout mice (GFP is green) shows no label for TRPM5 in GFP-

1253 positive MVCs (asterisks) and does show sparse labeling in the OSN nuclear layer (arrows). The

1254 scale bar is 20 µm.

1255

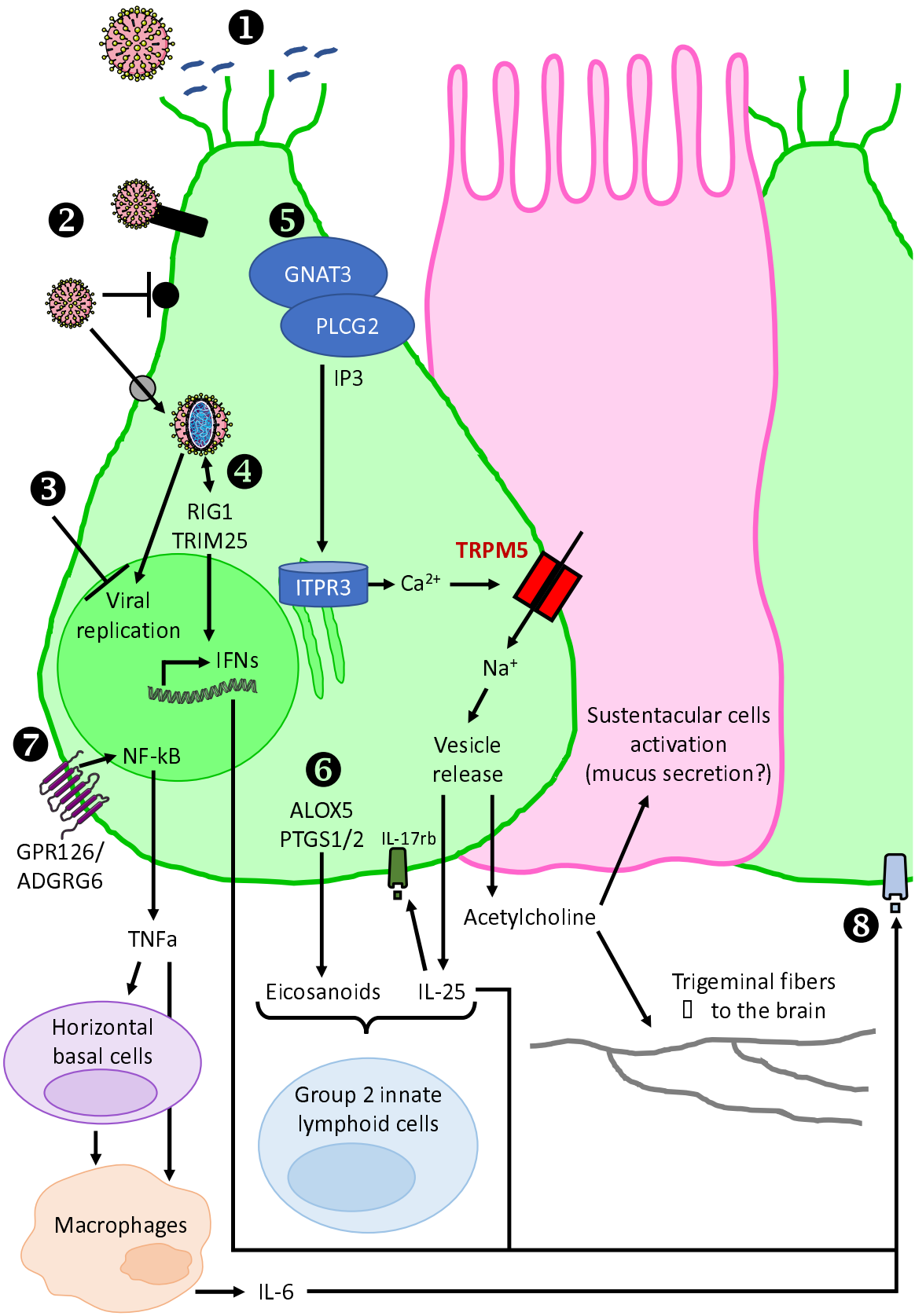

1256

Figure 6. Model depicting the role for microvillous cells involvement in the olfactory epithelium innate immune response to viral infection. 1) Secreted or cell surface glycoproteins constitute a first barrier preventing virus entry. 2) When reaching MVC_eGFP, viruses can encounter three types of membrane proteins: adhesion molecules that trigger intracellular signaling upon viral recognition (black rectangle), transmembrane proteins that block virus entry (black circle), viral receptors allowing virus entry (grey circle). 3) MVC_eGFP express numerous transcriptional factors involved in the inhibition of viral replication. 4) Cytosolic viral RNA sensing induces the production of type I interferons. 5) A possible signaling pathway leading to intracellular calcium increase, TRPM5 activation and Na^+-mediated vesicle release. Acetylcholine can activate neighboring sustentacular cells and underlying trigeminal fibers. 6) Eicosanoids synthesis, along with IL-25 production, can recruit and activate group 2 innate lymphoid cells, which are key controllers of type 2 inflammation. 7) GPR126 activation results in NFkB activation and TNFα production. TNFα can directly activate macrophages. TNFα also induces a change in the function of horizontal basal cells, switching their phenotype from neuroregeneration to immune defense. 8) Interferons and cytokines can in turn activate antiviral immune response in neighboring MVC_eGFP.

Supplemental Information

Transcriptional profiling reveals TRPM5-expressing cells involved in viral infection in the olfactory epithelium

B. Dnate' Baxter[1,2,‡], Eric D. Larson[3,‡], Paul Feinstein[4], Arianna Gentile Polese[1,2], Andrew N. Bubak[5], Christy S. Niemeyer[5], Laetitia Merle[1,2], Doug Shepherd[6], Vijay R. Ramakrishnan[3], Maria A. Nagel[5], and Diego Restrepo[1,2,*]

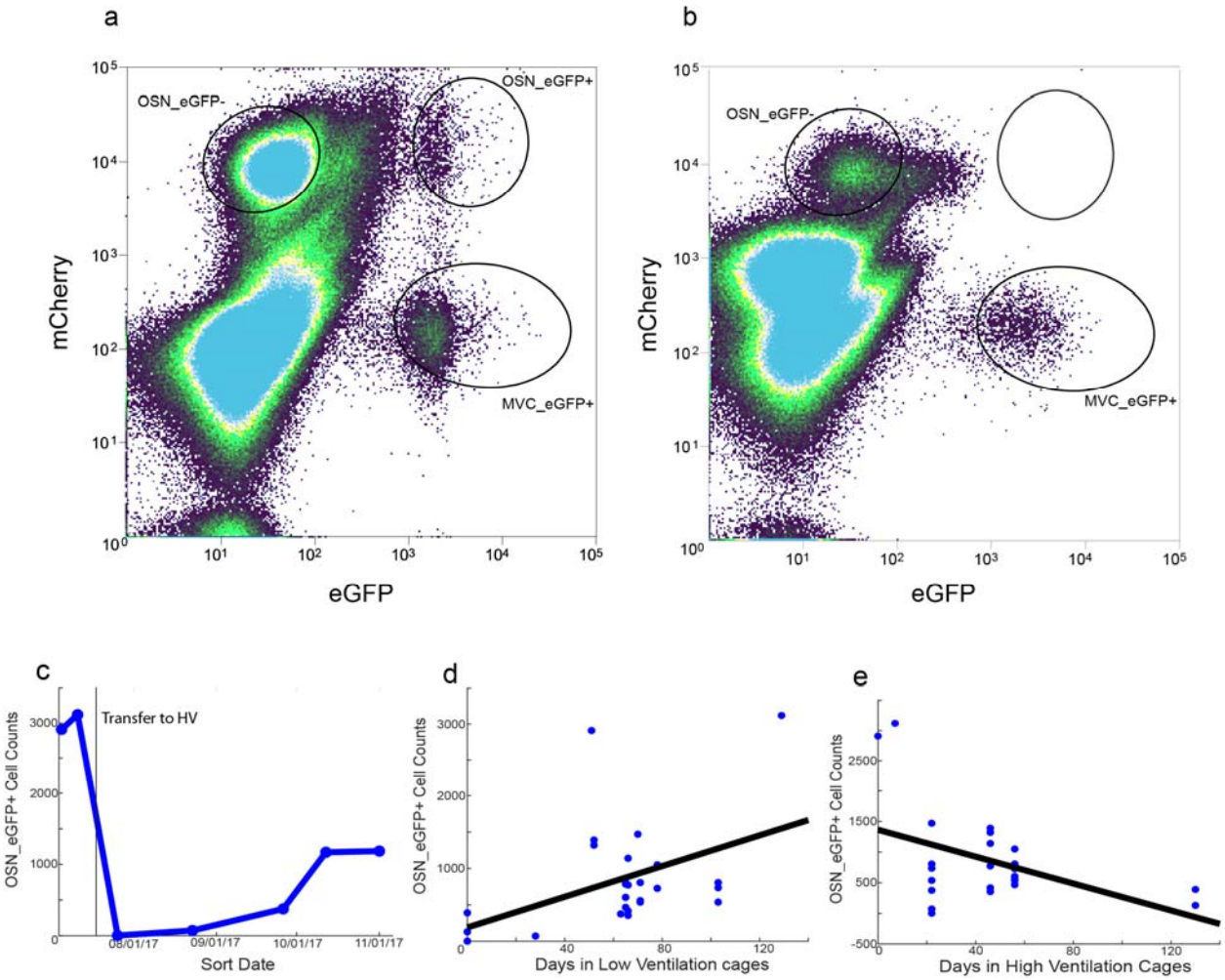

Figure 1, figure supplement 1. Decreased yield of OSN_eGFP+ cells when mice are moved from low ventilation (LV) to high ventilation (HV) cages.

a and b. Distribution of mCherry and eGFP fluorescence intensity for FACS-sorted cells that either were not transferred to HV cages (**a**) or were transferred to HV cages for 22 days before sorting (**b**).

c. Time course showing change in the number of sorted OSN_eGFP+s after mice were transferred to HV cages.

d and e. Dependence of the yield of OSN_eGFP+ cells after sorting on the number of days in LV cages (**d**) or the number of days in HV cages (**e**).

Figure 2 – figure supplement 1. Excel worksheet with the results of comparison of gene transcription between MVC_eGFP and OSN_EGFP-.

Figure 2 - figure supplement 2. Significant differences in gene ontology for MVC_eGFP+ compared to OSN_eGFP-.

Figure 2 - figure supplement 3. Metadata for the RNAseq.

1311

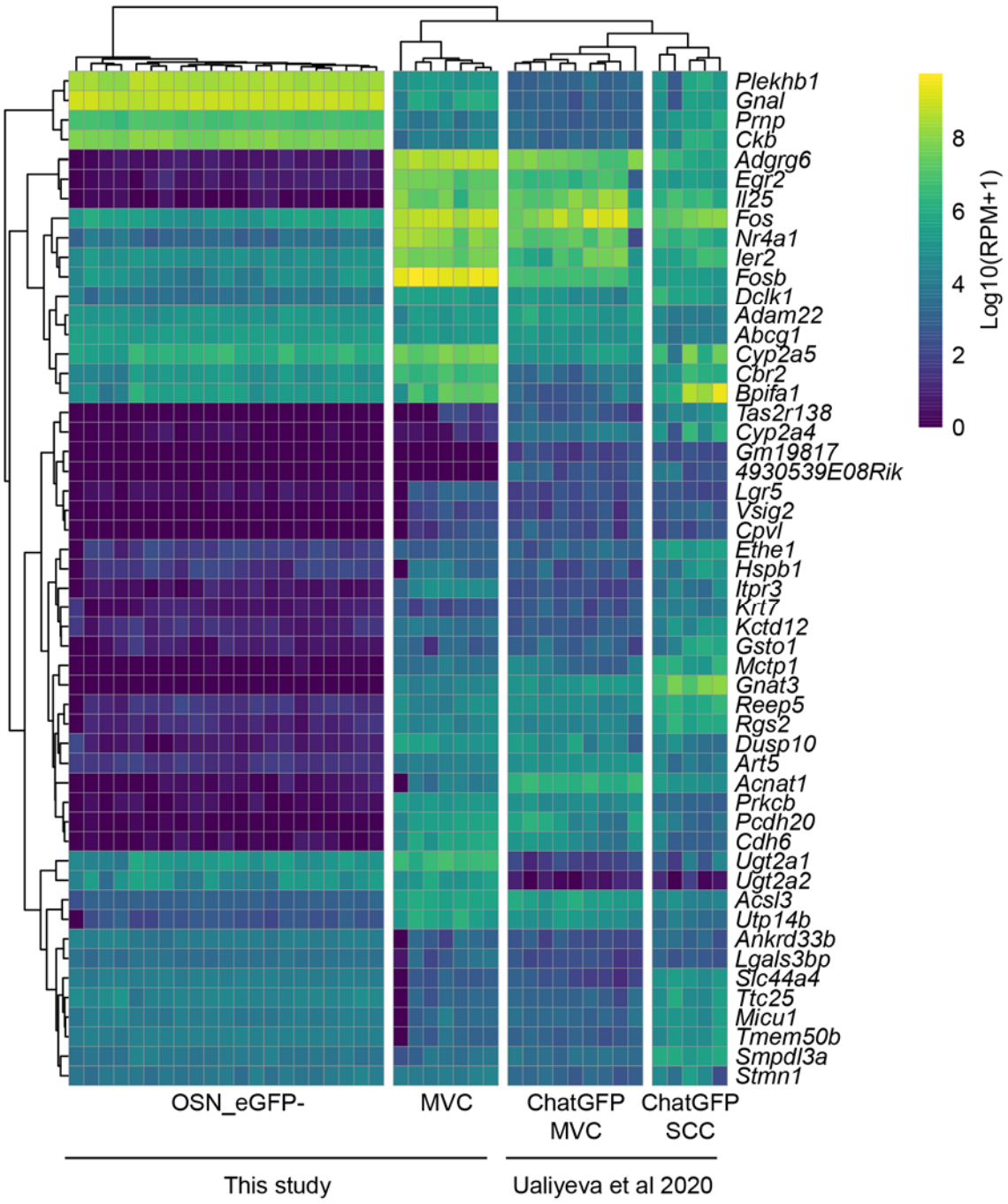

1312

1313 **Figure 2 – figure supplement 4.** Comparisons of gene expression between MVC_eGFP and

1314 OSN_eGFP- cells of this study and ChAT-eGFP MVCs and ChAT-eGFP SCCs profiled in the

1315 respiratory epithelium in the study of Ualiyeva and co-workers (Ualiyeva et al., 2020). This

1316 comparison is of limited value due to the fact that the gene profiling was performed in two

1317 separate studies.

1318

1319

Figure 3- figure supplement 1. Significant differences in inflammation gene ontology for MVC_eGFP+ compared to OSN_eGFP-.

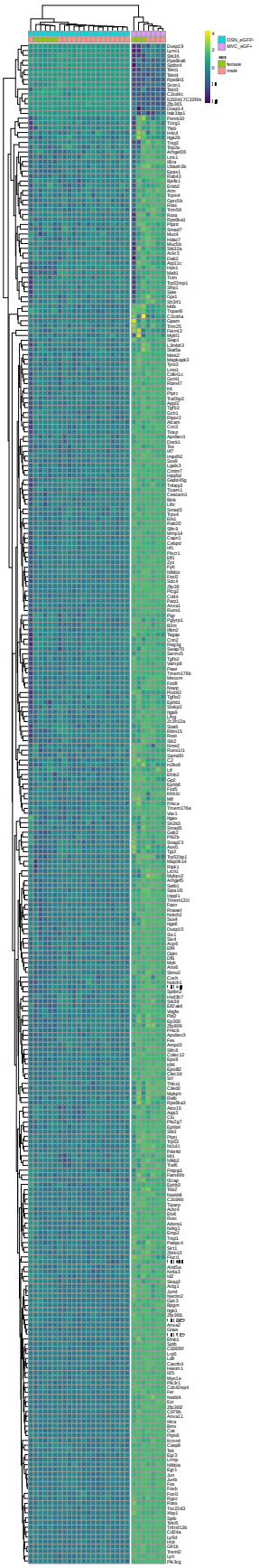

1323

1324 **Figure 3- figure supplement 2. Significant differences in immmunity gene ontology for**

1325 **MVC_eGFP+ compared to OSN_eGFP-.**

1326

Figure 4 – figure supplement 1. Excel worksheet with the results of comparison of gene transcription between OSN_EGFP+ and OSN_EGFP-.

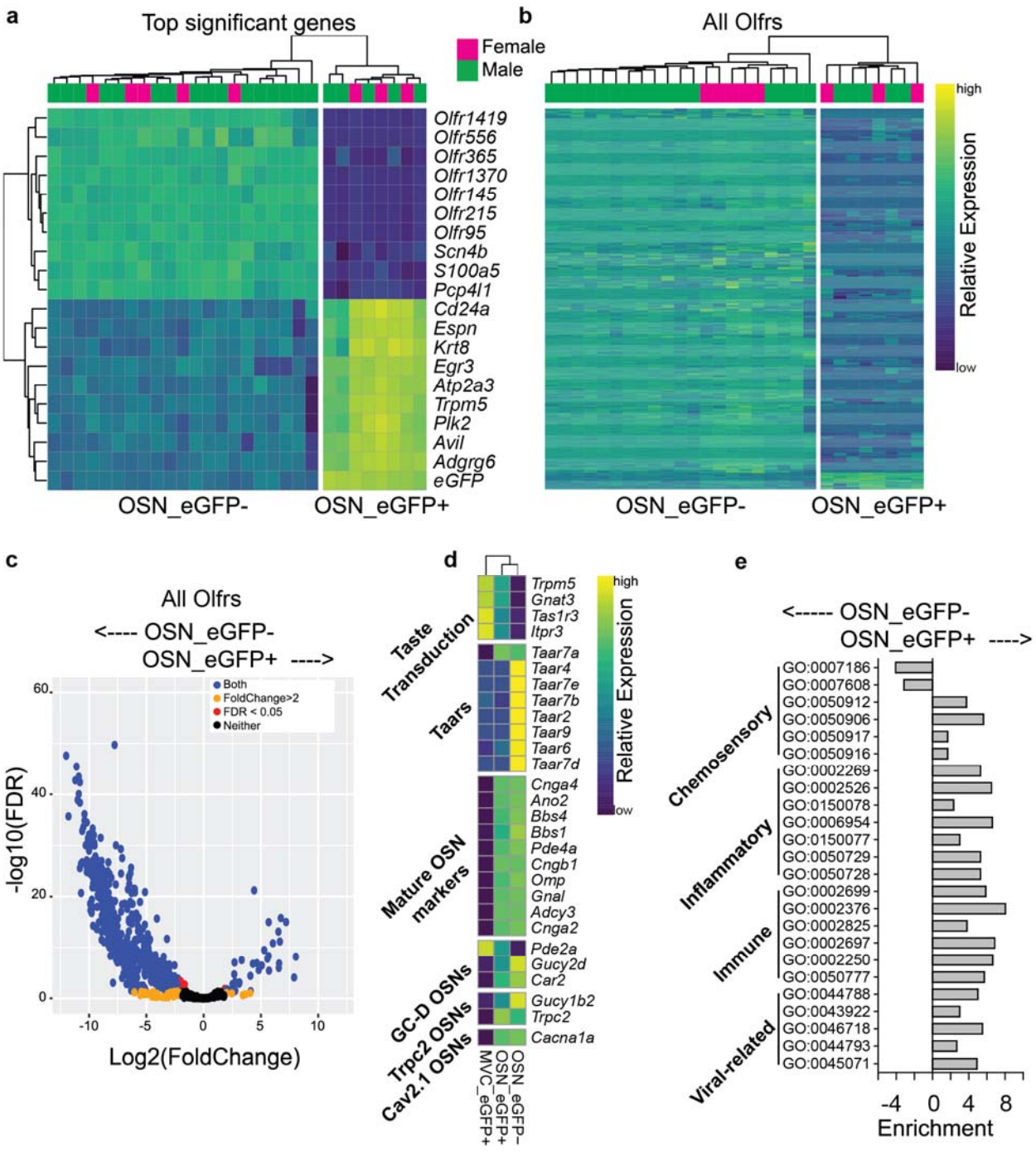

Figure 4 – figure supplement 2. RNAseq comparison of OSN_eGFP- and OSN_eGFP+ cells.

a. Heatmap showing the top 10 upregulated and top 10 downregulated genes identified by DESeq2.

b. Heatmap showing all *Olfr* genes detected in the data.

For both a and b, row and column order were determined automatically by the *pHeatmap* package in R. For each data point relative expression was calculated by subtracting the average row value from each individual value.

c. Volcano plot of all Olfactory receptors, demonstrating the small number of enriched olfactory receptors in the OSN_eGFP+ population.

d. Hierarchical clustering of transcripts for taste transduction and transcripts expressed in canonical and non-canonical OSNs identified by RNAseq as significantly different in expression between the cell groups. We compared expression of transcripts involved in taste transduction, canonical olfactory transduction, and non-canonical OSNs. The non-canonical OSNs considered here included guanilyl-cyclase D (GC-D) OSNs (Juilfs et al., 1997), Trpc2 OSNs (Omura and Mombaerts, 2014), Cav2.1 OSNs (Pyrski et al., 2018), and OSNs expressing trace amine-associated receptors (Taars) (Liberles, 2015). Transcripts identified by DESeq2.

e. Gene ontology (GO) term enrichment was calculated from differentially expressed genes using *TopGO* in R. An enrichment value for genes with Fischer p value <0.05 was calculated by dividing the number of expressed genes within the GO term by the number expected genes (by random sampling, determined by *TopGO*).

Figure 4 - figure supplement 3. Excel worksheet with the results of comparison of gene transcription between MVC_eGFP cells and OSN_eGFP+.

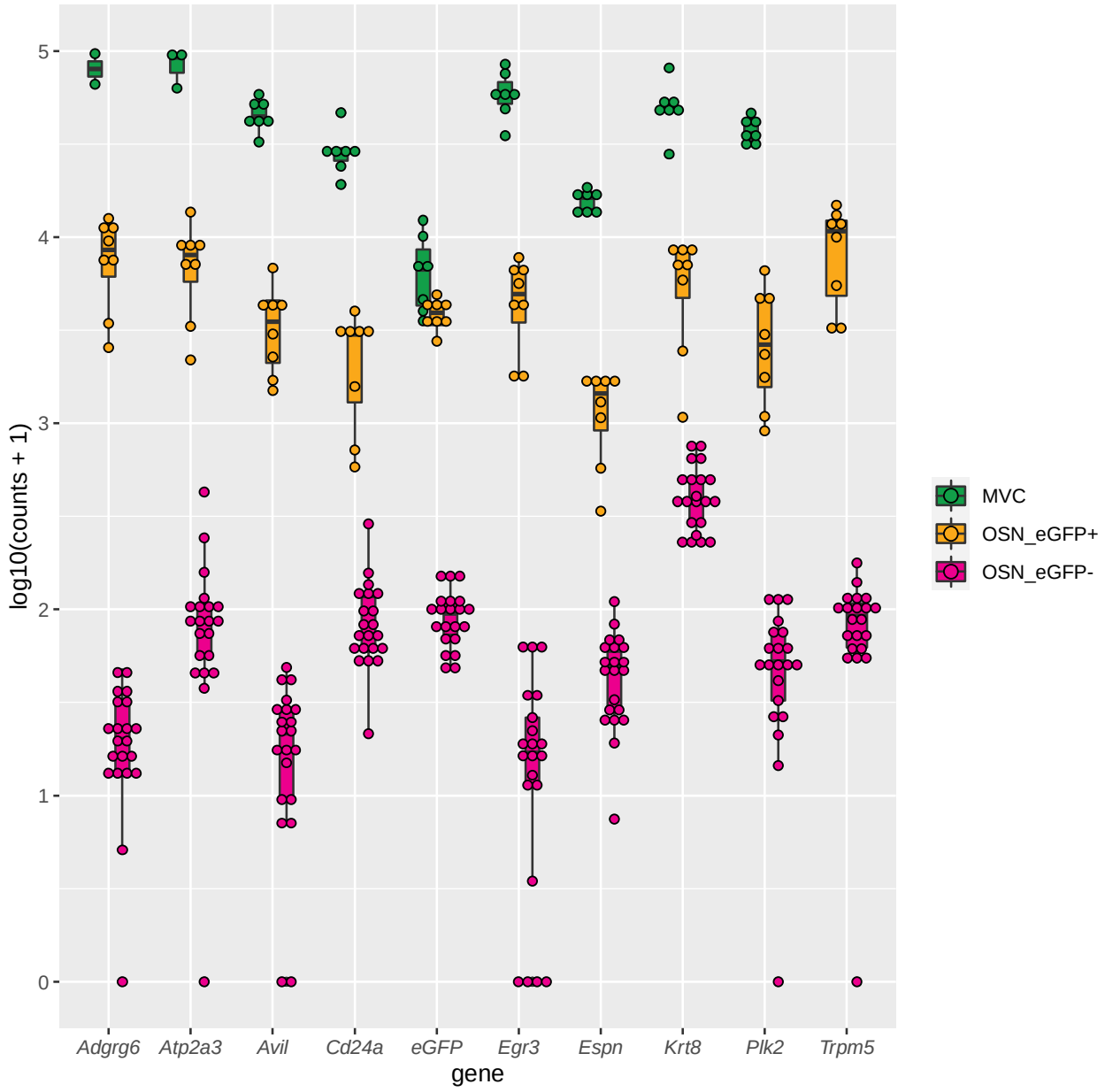

Figure 4 figure supplement 4. Boxplot showing expression levels for the top 10 genes that are significantly higher in OSN_eGFP+ vs. OSN_eGFP-.

Figure 4 - figure supplement 5. Excel worksheet with the results of genes whose transcription levels were significantly higher in OSN_eGFP+ compared to both MVC_eGFP cells and OSN_eGFP+.

Figure 4 figure supplement 6. GOnet analysis for the 80 genes whose transcription levels were significantly higher in OSN_eGFP+ compared to both MVC_eGFP cells and OSN_eGFP+. https://tools.dice-database.org/GOnet/job0c0357f0-d489-467d-adb7-9d33b52ff850/result

1372

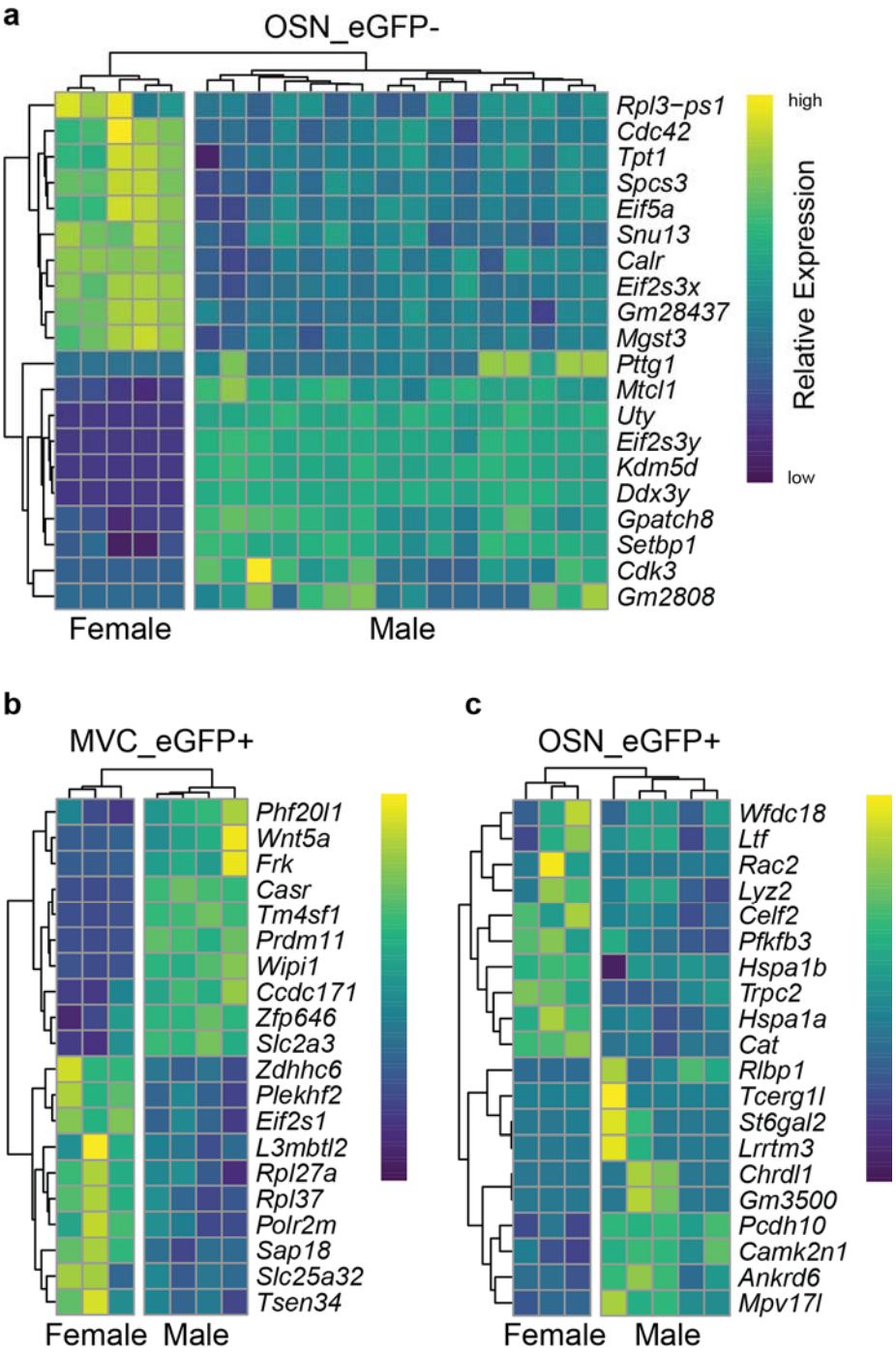

1373

1374 **Figure 4 – figure supplement 7. Hierarchical clustering of transcripts identified by RNAseq**

1375 **as significantly differentially expressed between male and female. a.** OSN_eGFP-. **b.**

1376 MVC_eGFP cells **c.** OSN_eGFP+. Transcripts identified by DESeq2.

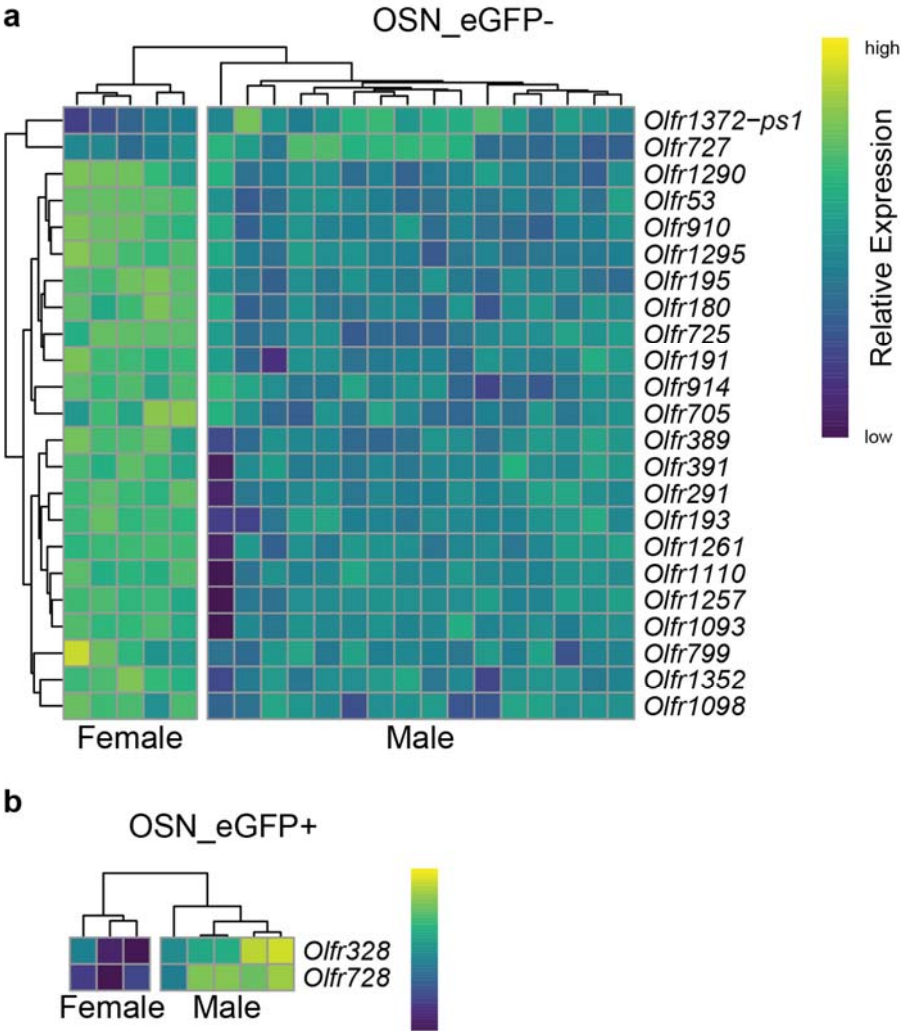

Figure 4 – figure supplement 8. Hierarchical clustering of olfactory receptor transcripts identified by RNAseq as significantly differentially expressed between male and female. a. OSN_eGFP-. **b.** OSN_eGFP+. Transcripts identified by DESeq2.

Figure 5 – figure supplement 1. Movie showing 3D rendering of HCR v3.0 *in situ* hybridization for TRPM5. Images were acquired with a high numerical aperture (NA) oblique plane microscope (Sapoznik et al., 2020). *In situ* is shown for TRPM5 (yellow) and OMP (green). DAPI is in blue.

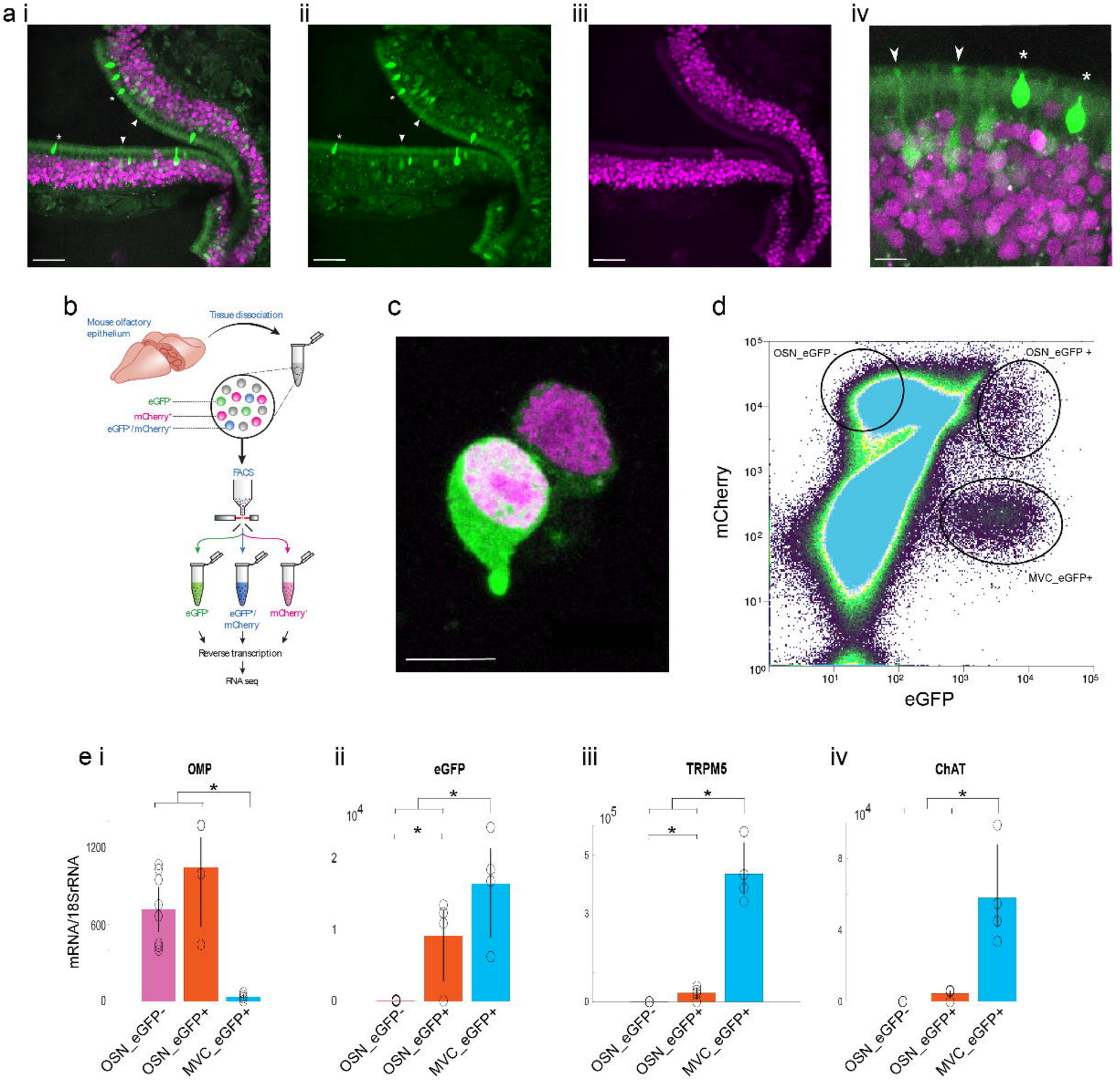
a i
ii
iii
iv
b
Mouse olfactory epithelium
Tissue dissociation
eGFP+
mCherry+
eGFP+/mCherry+
FACS
eGFP+
eGFP+/ mCherry+
mCherry+
Reverse transcription
RNA seq
c
d
OSN_eGFP -
OSN_eGFP +
MVC_eGFP+
mCherry
eGFP
e i
OMP
mRNA/18SrRNA
OSN_eGFP-
OSN_eGFP+
MVC_eGFP+
ii
eGFP
iii
TRPM5
iv
ChAT

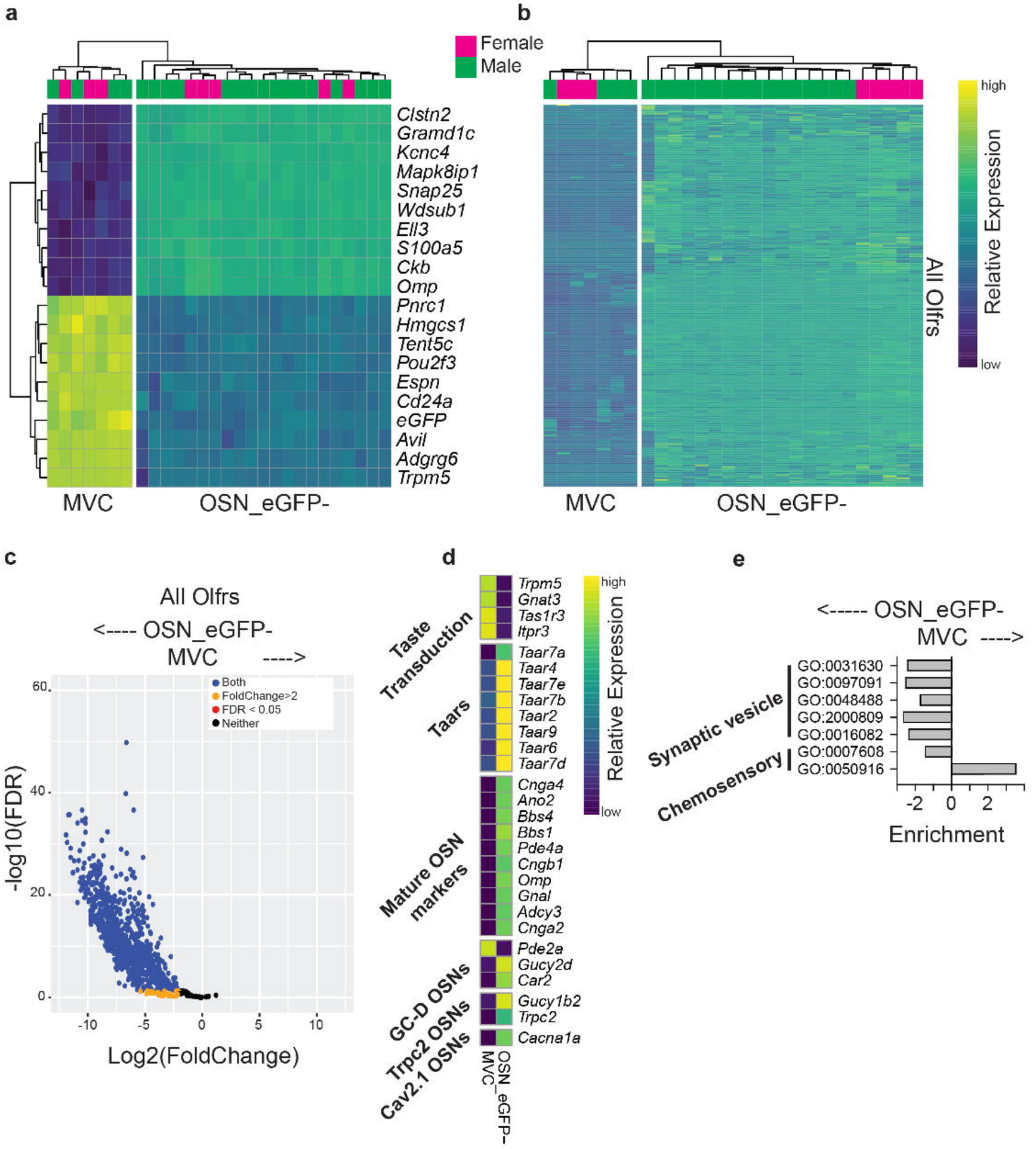
a
b
Female
Male
Clstn2
Gramd1c
Kcnc4
Mapk8ip1
Snap25
Wdsub1
Ell3
S100a5
Ckb
Omp
Pnrc1
Hmgcs1
Tent5c
Pou2f3
Espn
Cd24a
eGFP
Avil
Adgrg6
Trpm5
MVC
OSN_eGFP-
All Olfrs
high
low
Relative Expression
c
All Olfrs
<---- OSN_eGFP-
MVC ---->
Both
FoldChange>2
FDR < 0.05
Neither
-log10(FDR)
Log2(FoldChange)
d
Taste Transduction
Trpm5
Gnat3
Tas1r3
Itpr3
Taars
Taar7a
Taar4
Taar7e
Taar7b
Taar2
Taar9
Taar6
Taar7d
Mature OSN markers
Cnga4
Ano2
Bbs4
Bbs1
Pde4a
Cngb1
Omp
Gnal
Adcy3
Cnga2
GC-D OSNs
Pde2a
Gucy2d
Car2
Trpc2 OSNs
Gucy1b2
Trpc2
Cav2.1 OSNs
Cacna1a
MVC
OSN_eGFP-
e
<----- OSN_eGFP-
MVC ---->
Synaptic vesicle
GO:0031630
GO:0097091
GO:0048488
GO:2000809
GO:0016082
Chemosensory
GO:0007608
GO:0050916
Enrichment

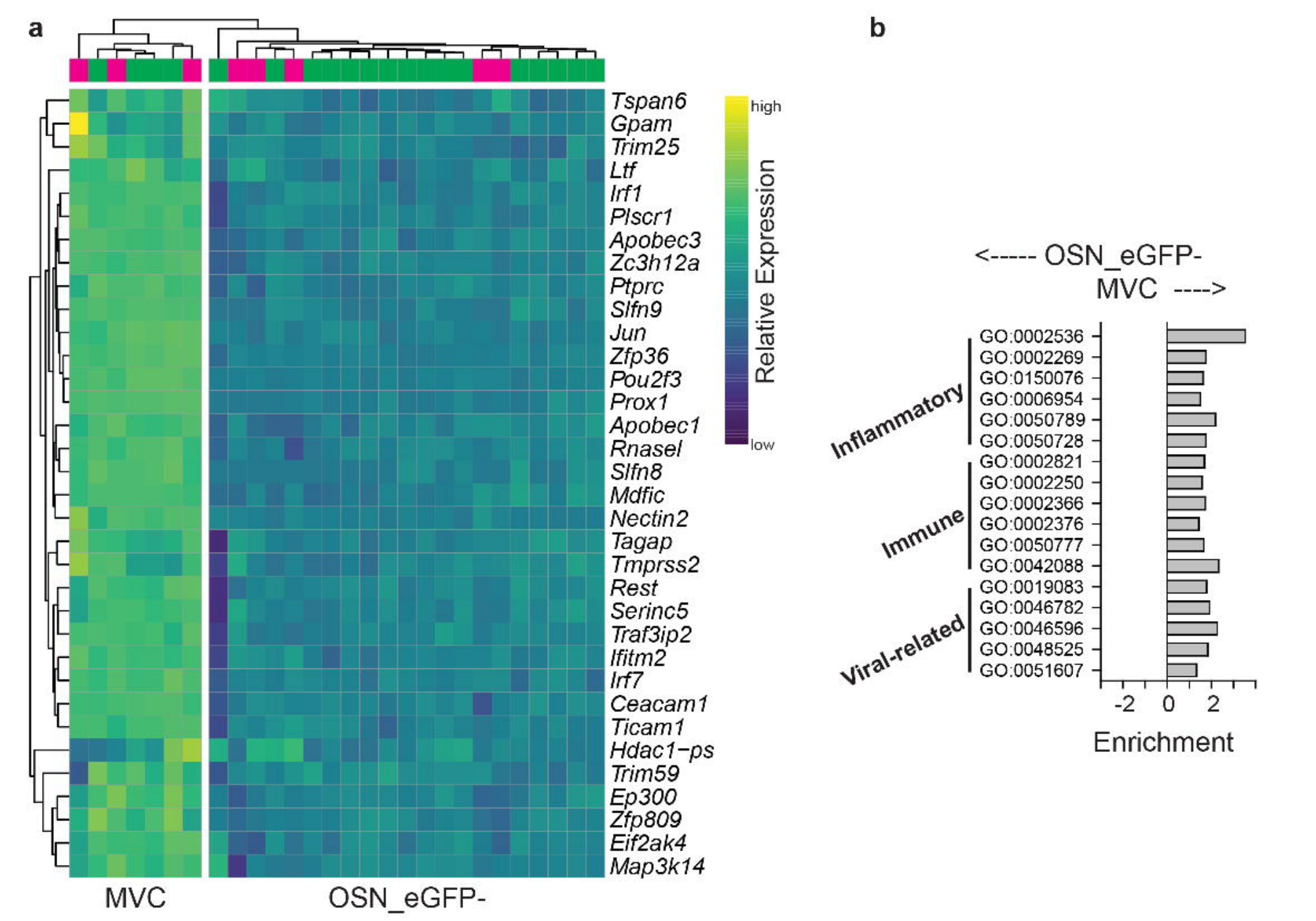
a
Tspan6
Gpam
Trim25
Ltf
Irf1
Plscr1
Apobec3
Zc3h12a
Ptprc
Slfn9
Jun
Zfp36
Pou2f3
Prox1
Apobec1
Rnasel
Slfn8
Mdfic
Nectin2
Tagap
Tmprss2
Rest
Serinc5
Traf3ip2
Ifitm2
Irf7
Ceacam1
Ticam1
Hdac1−ps
Trim59
Ep300
Zfp809
Eif2ak4
Map3k14
high
Relative Expression
low
MVC
OSN_eGFP-
b
<----- OSN_eGFP-
MVC ---->
Inflammatory
Immune
Viral-related
GO:0002536
GO:0002269
GO:0150076
GO:0006954
GO:0050789
GO:0050728
GO:0002821
GO:0002250
GO:0002366
GO:0002376
GO:0050777
GO:0042088
GO:0019083
GO:0046782
GO:0046596
GO:0048525
GO:0051607
-2
0
2
Enrichment

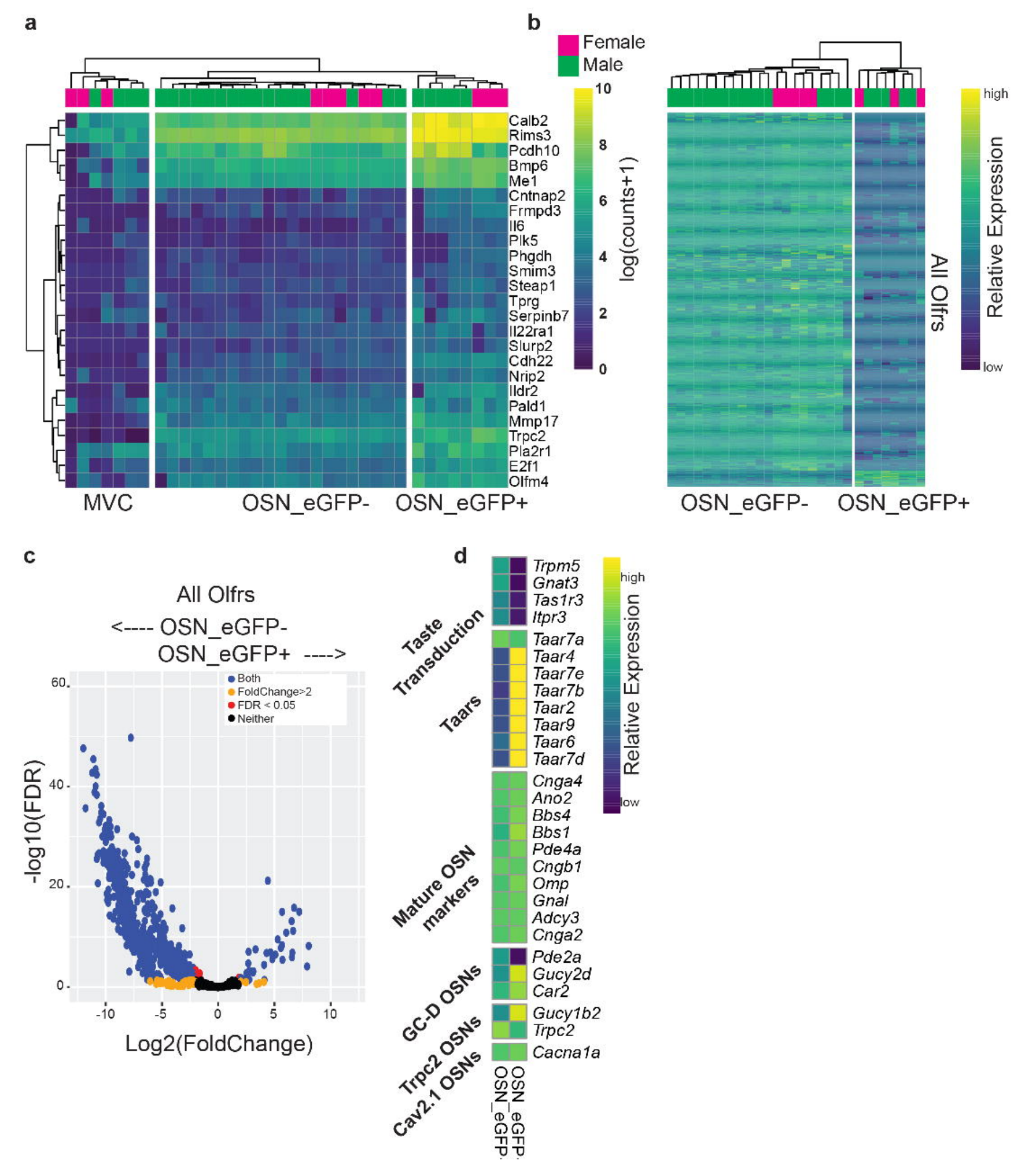
a
b
Female
Male
10
8
6
4
2
0
log(counts+1)
Calb2
Rims3
Pcdh10
Bmp6
Me1
Cntnap2
Frmpd3
Il6
Plk5
Phgdh
Smim3
Steap1
Tprg
Serpinb7
Il22ra1
Slurp2
Cdh22
Nrip2
Ildr2
Pald1
Mmp17
Trpc2
Pla2r1
E2f1
Olfm4
MVC
OSN_eGFP-
OSN_eGFP+
high
low
Relative Expression
All Olfrs
OSN_eGFP-
OSN_eGFP+
c
All Olfrs
<---- OSN_eGFP-
OSN_eGFP+ ---->
Both
FoldChange>2
FDR < 0.05
Neither
60
40
20
0
-log10(FDR)
-10
-5
0
5
10
Log2(FoldChange)
d
Taste Transduction
Trpm5
Gnat3
Tas1r3
Itpr3
Taars
Taar7a
Taar4
Taar7e
Taar7b
Taar2
Taar9
Taar6
Taar7d
Mature OSN markers
Cnga4
Ano2
Bbs4
Bbs1
Pde4a
Cngb1
Omp
Gnal
Adcy3
Cnga2
GC-D OSNs
Pde2a
Gucy2d
Car2
Trpc2 OSNs
Gucy1b2
Trpc2
Cav2.1 OSNs
Cacna1a
high
low
Relative Expression
OSN_eGFP-
OSN_eGFP+

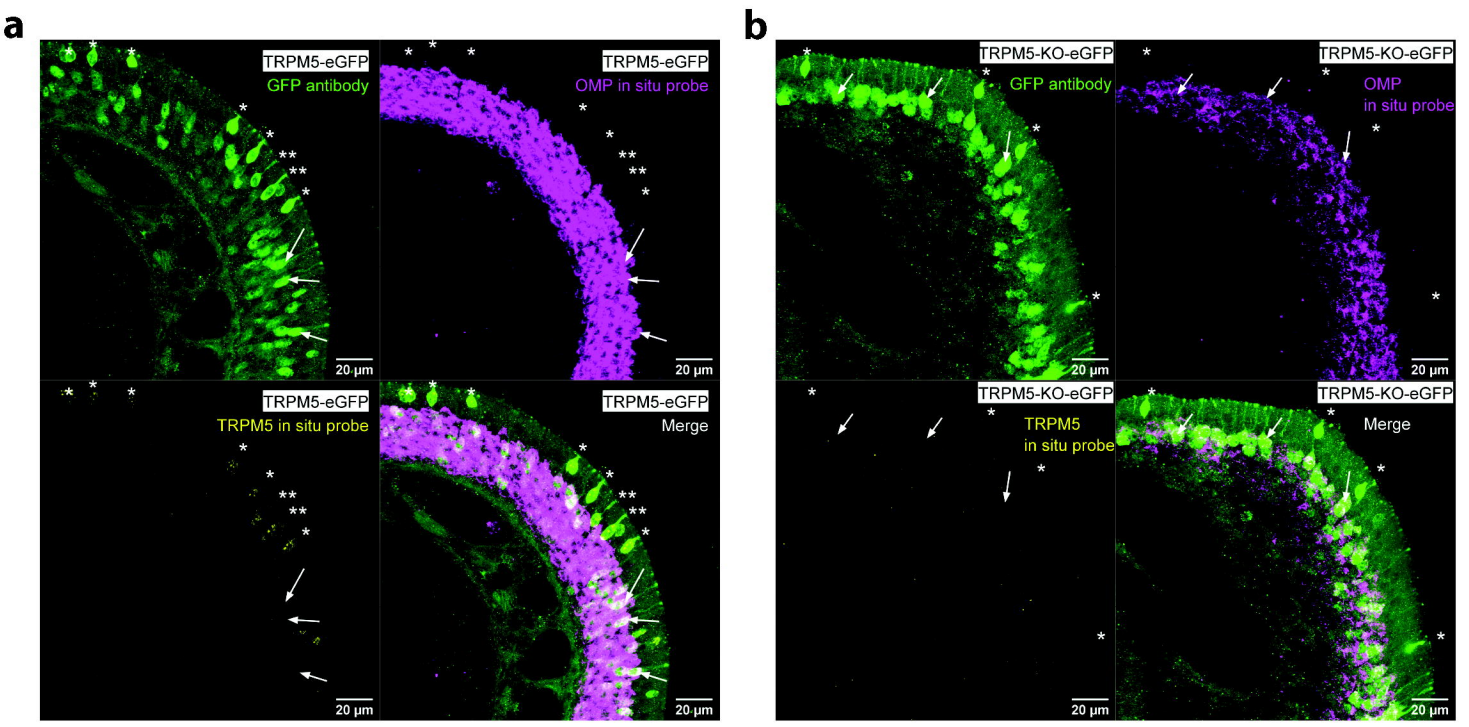
a
TRPM5-eGFP
GFP antibody
20 μm
TRPM5-eGFP
OMP in situ probe
20 μm
TRPM5-eGFP
TRPM5 in situ probe
20 μm
TRPM5-eGFP
Merge
20 μm
b
TRPM5-KO-eGFP
GFP antibody
20 μm
TRPM5-KO-eGFP
OMP
in situ probe
20 μm
TRPM5-KO-eGFP
TRPM5
in situ probe
20 μm
TRPM5-KO-eGFP
Merge
20 μm

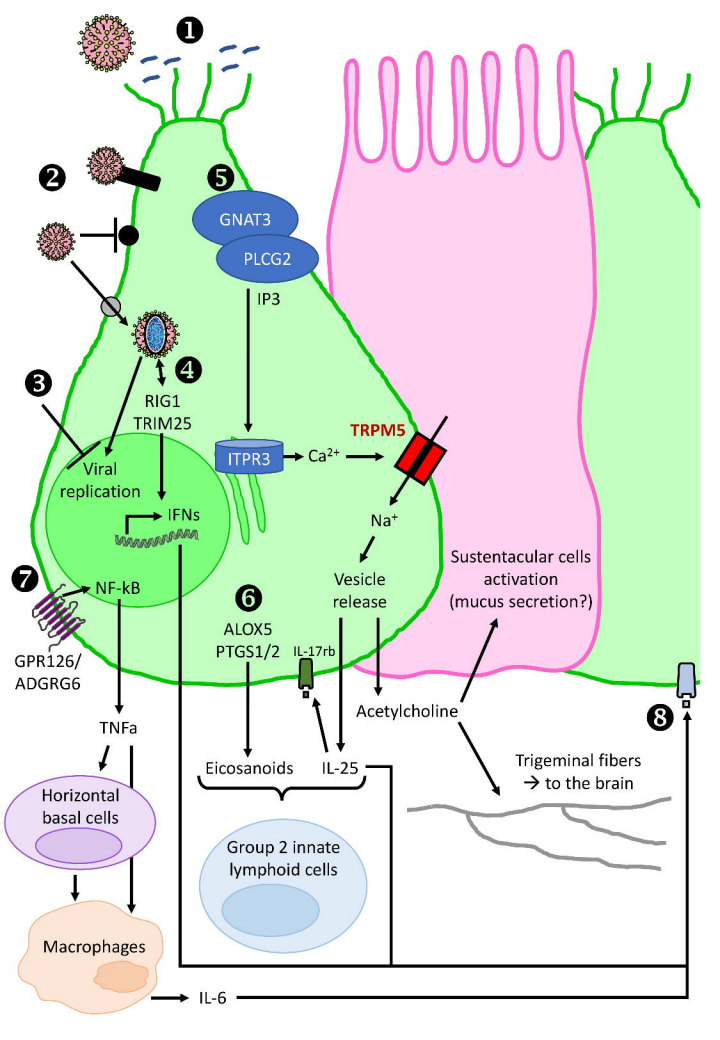
1
2
3
4
5
6
7
8
GNAT3
PLCG2
IP3
RIG1
TRIM25
Viral replication
IFNs
ITPR3
Ca2+
TRPM5
Na+
Vesicle release
Sustentacular cells activation (mucus secretion?)
NF-kB
GPR126/ ADGRG6
ALOX5 PTGS1/2
IL-17rb
Acetylcholine
TNFa
Eicosanoids
IL-25
Trigeminal fibers → to the brain
Horizontal basal cells
Group 2 innate lymphoid cells
Macrophages
IL-6